

**A STUDY OF DOMAIN WALLS IN UNIAXIAL MAGNETIC MATERIALS**

**A STUDY OF DOMAIN WALLS  
IN UNIAXIAL MAGNETIC MATERIALS**

**by**

**Magid Y. Dimyan, B.Sc. (Cairo),  
M.Eng. (McMaster)**

**A Thesis**

**Submitted to the Faculty of Graduate Studies  
in Partial Fulfilment of the Requirements**

**for the Degree**

**Doctor of Philosophy**

**McMaster University**

**May 1972**

DOCTOR OF PHILOSOPHY (1972)  
(Electrical Engineering)

McMaster University  
Hamilton, Ontario

TITLE: A Study of Domain Walls in Uniaxial Magnetic Materials

AUTHOR: Magid Y. Dimyan, B.Sc. (Cairo)  
M.Eng. (McMaster University)

SUPERVISOR: Professor E. Della Torre

NUMBER OF PAGES: (xi), 79

SCOPE AND CONTENTS:

A study of domain walls in some uniaxial magnetic materials is reported. Methods for measuring some important material parameters in the rare-earth orthoferrites and the uniaxial garnets are described. The temperature sensitivities of bubble domains in orthoferrites and garnets are derived in terms of the material parameters and conditions for minimum and zero temperature sensitivities are obtained. An investigation of the current requirement to cut a bubble domain from a strip or another bubble domain is also reported.

## ABSTRACT

An investigation of domain walls in some uniaxial magnetic materials is reported in this thesis. Firstly, a method for measuring the wall energy anisotropy in orthoferrites, which causes cylindrical magnetic (bubble) domains to be elliptical is described. In  $\text{Sm}_{0.55}\text{Tb}_{0.45}\text{FeO}_3$  a measured anisotropy energy of 1.7% of the wall-energy density at room temperature is responsible for eccentricities as large as 0.4 at average bubble radii equal to 85% of the bubble strip-domain transition radius. The relationship between material parameters and wall-energy anisotropy is discussed. The hypothesis that in orthoferrites walls parallel to the a axis are Bloch walls while walls parallel to the b axis are Néel walls is investigated by measuring the wall anisotropy as a function of the quality factor of the material by varying the temperature of the sample. The measurements seem to verify the predicted dependence of wall anisotropy on the quality factor and thus the hypothesis.

A method for measuring the temperature dependence of the wall-energy density in orthoferrites and the saturation magnetization in garnets is described. The advantage of the method is that it uses a single isolated bubble domain without the need to destroy the bubble in order to obtain the measurements. This method led to the derivation of the temperature sensitivities of bubble domains in orthoferrites and garnets in terms of the material parameters. Optimum plate thicknesses to minimize the variation of bubble diameter with temperature are

considered. Also, the condition for zero temperature sensitivity of bubbles in some uniaxial materials is derived in terms of the material parameters.

Finally, a study of the current requirement to cut a bubble domain from a strip domain or another bubble in uniaxial plates is reported in this thesis.

### ACKNOWLEDGEMENTS

The author particularly wishes to express his sincere gratitude to Dr. E. Della Torre for his helpful advice, criticism and encouragement received during the course of this work. Thanks are also due to Dr. A.S. Gladwin and Dr. B.K. Garside, the other members of the Supervisory Committee, for their interest in the investigation.

The author is grateful to the Bell Telephone Laboratories, Inc., and Bell-Northern Research for supplying the orthoferrite samples.

Thanks are due to the National Research Council of Canada and McMaster University for financial support in the form of a McMaster Assistantship and a University Scholarship.

Finally, the author wishes to thank Mrs. Kathy Paulin for typing the thesis on such short notice.

## TABLE OF CONTENTS

|  | <u>Page</u> |
|--|-------------|
| CHAPTER I - INTRODUCTION   | 1           |
| 1.1 General  | 1           |
| 1.2 Outline of the Thesis  | 2           |
| <br>   |             |
| CHAPTER II - A REVIEW OF BUBBLE DOMAIN MATERIALS, DEVICES AND STABILITY  | 5           |
| 2.0 Introduction   | 5           |
| 2.1 Bubble Materials   | 6           |
| 2.2 Bubble Devices   | 10          |
| 2.3 The Theory of Stability of Bubble Domains  | 12          |
| 2.4 Measurement Techniques   | 19          |
| 2.5 Measuring Equipment  | 22          |
| <br>   |             |
| CHAPTER III - ANISOTROPY OF WALL ENERGY IN ORTHOFERRITES   | 25          |
| 3.0 Introduction   | 25          |
| 3.1 Wall Anisotropy  | 25          |
| 3.2 Bubble Ellipticity as a Function of Radius   | 27          |
| 3.3 Experimental Methods and Results   | 31          |
| 3.4 Conclusions  | 40          |
| <br>   |             |
| CHAPTER IV - TEMPERATURE SENSITIVITY OF BUBBLE DOMAINS   | 41          |
| 4.0 Introduction   | 41          |
| 4.1 A Method for Measuring the Temperature Dependence of $\sigma_w$ and $q$ in the Mixed Rare-Earth Orthoferrites. | 41          |
| 4.2 A Method for Measuring the Temperature Dependence of $M_S$ in Uniaxial Garnets                                 | 44          |
| 4.3 Temperature Sensitivity  | 45          |
| 4.4 Zero Temperature Sensitivity of Bubbles  | 48          |
| 4.5 Conclusions  | 50          |
| <br>   |             |
| CHAPTER V - CUTTING STRIP AND BUBBLE DOMAINS   | 54          |
| 5.0 Introduction   | 54          |
| 5.1 Cutting Strip Domains by Use of Electric Currents  | 54          |
| 5.2 Replication of Bubble Domains  | 61          |

|                          | <u>Page</u> |
|--------------------------|-------------|
| CHAPTER V - Continued    |             |
| 5.3 Conclusions          | 69          |
| CHAPTER VI - CONCLUSIONS | 70          |
| REFERENCES               | 73          |

## LIST OF FIGURES

| <u>Figure</u> |   | <u>Page</u> |
|---------------|---|-------------|
| 2.1           | A two-sublattice model of the spin arrangement in an orthoferrite orthorhombic cell.  | 8           |
| 2.2           | Magnetic domain configuration and coordinate system.  | 14          |
| 2.3           | Magnetostatic force, radial and elliptical stability functions.   | 17          |
| 2.4           | Bubble collapse and run-out diameters as a function of plate thickness.   | 20          |
| 2.5           | The observation of domains in uniaxial magnetic materials. Inset: Strip and bubble domains in a plate of $\text{Sm}_{0.55}\text{Tb}_{0.45}\text{FeO}_3$ , as viewed using the Faraday effect (magnification x40). | 24          |
| 3.1           | Illustration of geometry chosen to describe an elliptical domain.   | 28          |
| 3.2           | Eccentricity of the elliptical domain as a function of bubble radius.   | 32          |
| 3.3           | Measurement of wall energy anisotropy as a function of domain aspect ratio.   | 34          |
| 3.4           | Illustration of technique for measuring the anisotropy field at room temperature using curves of magnetization versus field.  | 36          |
| 3.5           | The quality factor as a function of temperature obtained from vibrating sample magnetometer measurements.   | 37          |
| 3.6           | Measurements of $\sigma_x/\sigma_a$ as a function of the temperature of the sample.   | 39          |
| 4.1           | The temperature sensitivities of bubble diameters for the mixed rare-earth orthoferrites and the uniaxial garnets as a function of plate thickness for two bias conditions.                                       | 47          |

| <u>Figure</u> |   | <u>Page</u> |
|---------------|---|-------------|
| 4.2           | The ratio of the fractional changes in wall energy density and magnetization for zero temperature sensitivity as a function of plate thickness for two bias conditions.           | 51          |
| 4.3           | $(\Delta\sigma_w/\sigma_w)/(\Delta M_S/M_S)$ as a function of bubble diameter for several plate thicknesses.  | 52          |
| 5.1           | Experimental and theoretical cutting field as a function of half strip width for a $6\ell_M$ thick plate of $TbFeO_3$ , and an $8\ell_M$ thick plate of $Sm_{0.55}Tb_{0.45}FeO_3$ | 56          |
| 5.2           | Shape of strip domain at instant of cutting.  | 60          |
| 5.3(a)        | Cutting field as a function of notch width for $h=8\ell_M$ and $b=h$ at point O in Fig. 5.2.  | 62          |
| 5.3(b)        | Cutting field as a function of notch width for $h=8\ell_M$ and $b=h$ at point P in Fig. 5.2.  | 63          |
| 5.4           | $c/b$ as a function of $b/h$ for $h=6\ell_M, 8\ell_M$ .   | 64          |
| 5.5           | Shape of bubble domain at instant of cutting.   | 66          |
| 5.6           | Bubble replication field as a function of $b/h$ for two plate thicknesses.  | 67          |
| 5.7           | Bubble replication field as a function of plate thickness.  | 68          |

## LIST OF SYMBOLS

|                   |  |
|-------------------|--|
| $H$               | : Applied bias field   |
| $\sigma_w$        | : Wall energy density per unit area  |
| $M_s$             | : Saturation magnetization   |
| $h$               | : Plate thickness  |
| $\ell_M$          | : Characteristic material length   |
| $K_u$             | : Uniaxial anisotropy constant   |
| $r_b(\theta)$     | : Bubble shape in the plane of the uniaxial platelet   |
| $r_0$             | : Average bubble radius  |
| $d$               | : Average bubble diameter  |
| $\Delta r_n$      | : Small variation in domain size   |
| $\Delta \theta_n$ | : Small variation in domain shape  |
| $\Delta E_T$      | : Total energy variation of bubble domain  |
| $E_T$             | : Total domain energy  |
| $E_w$             | : Total wall energy  |
| $E_H$             | : Interaction energy with external field   |
| $E_M$             | : Internal magnetostatic energy  |
| $a$               | : Domain aspect ratio  |
| $F(a)$            | : Magnetostatic force function   |
| $S_0(a)$          | : Radial stability function  |
| $S_2(a)$          | : Elliptical stability function  |
| $\sigma_B$        | : Bloch wall energy density  |
| $\sigma_N$        | : Néel wall energy density   |
| $A_b/A_a$         | : Ratio of exchange constants separated by displacement along the b and a axis, respectively |

|                  |   |  |
|------------------|---|--|
| $q$              | : | Quality factor   |
| $\sigma_m$       | : | Wall energy density when wall lies along easy axis       |
| $\sigma_x$       | : | Wall-energy anisotropy                                   |
| $\alpha$         | : | Angle between wall direction and hard direction          |
| $\theta$         | : | Angle between radius vector and easy direction           |
| $\beta$          | : | Angle between tangent line and normal to radius vector   |
| $r_2$            | : | Second-order variation from circle                       |
| $\sigma_a$       | : | Average wall energy density                              |
| $e$              | : | Eccentricity of elliptical domain                        |
| $\Delta\sigma_w$ | : | Incremental increase in wall energy density              |
| $\Delta d$       | : | Incremental increase in diameter of bubble               |
| $\Delta M_s$     | : | Incremental increase in saturation magnetization         |
| $\Delta q$       | : | Incremental increase in quality factor                   |
| $S$              | : | Temperature sensitivity of bubble diameter               |
| $\Delta T$       | : | Change in temperature                                    |
| $\bar{H}_z$      | : | Average magnetic field on domain wall                    |
| $I$              | : | Current flowing in wire                                  |
| $r$              | : | Radius of wire   |
| $a$              | : | Horizontal distance from center of wire                  |
| $H_r$            | : | Cutting field  |
| $I_r$            | : | Cutting current  |
| $2b$             | : | Strip domain width                                       |
| $f(x)$           | : | Equation of domain wall shape                            |
| $\bar{H}_M$      | : | Average value of magnetic field due to magnetization     |
| $H_{eq}$         | : | Equivalent field to overcome pressure due to wall energy |
| $R$              | : | Radius of curvature at point of cutting                  |

## CHAPTER 1

### INTRODUCTION

#### 1.1 General

Since the advent of the electronic computer and other data-processing devices, a continuous effort has been made to improve the speed, capacity and reliability of these devices' memory systems. The fastest and most flexible memory systems at present are those using either ferrite cores or solid state integrated circuit chips. At the moment, cores are cheaper, costing approximately one cent per bit of storage capacity. However, it is obvious that for mass memories exceeding  $10^{10}$  bits the cost would be prohibitive. Magnetic-disk memory systems, currently being used for high-capacity storage, are somewhat unreliable since these systems depend on the mechanical movement of a thin magnetic film on which the information is stored. Moreover, one cannot manipulate the stored information without reading it out and writing it in again, a process that can take appreciable time. Thus, the search for faster, cheaper and more reliable memories has led to a new technology in which data bits are stored in the form of magnetic "bubbles" moving in thin films or wafers of magnetic material. The bubbles are stable over a considerable range of conditions and can be moved in two dimensions at very high velocity.

The evidence available at the present time indicates that bubble memories should be substantially cheaper than core memories (costing an estimated few millicents per bit of information stored) and several times

faster than magnetic-disk memory systems. Also, in bubble devices one can perform many logical operations on the stored data without reading them out and writing them back in. Finally, since bubble devices have no moving parts they are expected to work reliably for many years.

## 1.2 Outline of the Thesis

A study of domain walls in uniaxial magnetic materials has been carried out and is reported in this thesis. The purpose of the study is to gain a better understanding of the structure and properties of uniaxial materials that support cylindrical magnetic domains, and to develop methods for measuring important material parameters.

Cylindrical magnetic domains often referred to as bubbles, have device applications as discussed in Chapter II. Thus, the properties of magnetic materials that support bubble domains are reviewed with special emphasis given to the single and mixed rare-earth orthoferrites and the uniaxial garnets. Methods for growing and processing these materials are briefly discussed. A discussion of the various techniques employed to generate, propagate and detect bubbles in devices is given. The theory of static stability of bubble domains in uniaxial platelets or films, which is very important in the design of bubble devices, is summarized. Some of the results of the theory are used in Chapters III and IV. Methods for measuring some relevant material parameters that make use of the optical Faraday effect are also described in this Chapter.

The original contributions made by the author are reported in Chapters III, IV and V. In order to gain a better understanding of

domain walls in uniaxial materials, the influence of three effects on the domain walls have been investigated. These are: Wall-energy anisotropy, temperature and electric currents.

In Chapter III, the anisotropy of wall energy in orthoferrites, which tends to distort otherwise circular domains into elliptical domains, is discussed. A method for measuring this wall anisotropy which depends on simply measuring the eccentricity of the elliptical domain as a function of mean bubble radius is developed and is used to measure the wall anisotropy in samarium-terbium orthoferrite ( $\text{Sm}_{0.55}\text{Tb}_{0.45}\text{FeO}_3$ ). In attempting to explain wall-energy anisotropy, it is suggested that there are two effects giving rise to this anisotropy: a difference in exchange interaction along the two hard magnetocrystalline axes, and a difference in the types of walls along different axes. Thus, when the wall lies along the a axis, a Bloch wall results, however, when the wall lies along the b axis, the magnetization cannot rotate through a very hard b axis and a Néel wall results. This hypothesis is verified by subjecting a sample of  $\text{Sm}_{0.55}\text{Tb}_{0.45}\text{FeO}_3$  to a temperature test and measuring the wall-anisotropy as described in Chapter III.

A method suitable for measuring the temperature dependence of the wall energy density in the mixed rare-earth orthoferrites and the saturation magnetization in some uniaxial garnets is presented in Chapter IV. Most of the methods for measuring the wall-energy and the magnetization reviewed in Chapter II require the collapse of a bubble domain. The main advantage of the method described in this Chapter is that it only requires a single isolated bubble domain without the need to destroy the bubble in order to obtain the measurement. The temperature sensitivities

of bubble diameter in orthoferrite and garnet wafers are also derived in terms of the material parameters. Optimum plate thicknesses to minimize the variation of bubble diameter with temperature in orthoferrites and garnets are obtained. It is shown that it is possible to obtain zero temperature sensitivity of bubbles in some uniaxial materials. Curves are provided that can be used in designing bubble devices having fixed bubble sizes.

In order to gain some insight in the generation of bubble domains in devices, a study of the current requirement to cut a bubble from a strip domain was carried out both experimentally and theoretically and presented in Chapter V. The strip domains in  $\text{Sm}_{0.55}\text{Tb}_{0.45}\text{FeO}_3$  and  $\text{TbFeO}_3$  plates were cut by use of a pulsed current flowing through a fine wire touching the plate surfaces and placed at right angles to the domain walls. Various functions were used to simulate the shape of the walls at the instant of cutting. It is found that good agreement with the measured values of cutting field is obtained when the wall shape is considered to consist of sections of ellipses. A theoretical study of the fields required to replicate bubbles has also been carried out and the results are also given in Chapter V.

## CHAPTER II

### A REVIEW OF BUBBLE DOMAIN MATERIALS, DEVICES AND STABILITY

#### 2.0 Introduction

Cylindrical magnetic domains, or bubbles, were first observed by Kooy and Enz<sup>31</sup> in 1960 in thin barium ferrite wafers. They have recently received considerable attention because of possible device applications. Bobeck<sup>4</sup> demonstrated in 1967 that isolated bubble domains in uniaxial magnetic platelets or films can be manipulated to perform memory, logic and transmission functions. This work stimulated research in bubble materials and devices<sup>5,10</sup> as well as in the stability of these domains as a function of material parameters and geometry<sup>44,45,46</sup>. At present, the prospect of utilizing magnetic bubble devices to provide large-capacity information storage of high reliability at very low cost appears promising. Thus, bubble shift registers with storage densities exceeding  $2.5 \times 10^6$  bits/in<sup>2</sup> and with data-processing rates up to  $10^6$  bits/sec have been built<sup>7</sup>. Also, a design of a highly reliable  $10^8$ -bit bubble domain mass memory has been proposed<sup>3</sup>.

In this Chapter, a brief review of bubble materials and devices is presented. The theory of static stability of bubble domains and the methods for measuring important material parameters are briefly discussed.

## 2.1 Bubble Materials

Bubble domains can exist in single crystal, low magnetic moment, essentially uniaxial magnetic materials when the crystal is cut into thin platelets, with the easy axis of magnetization perpendicular to the platelet surface. When the anisotropy field of the material is larger than the moment of the material the magnetization will lie along the easy axis. Materials in which bubbles have been observed include ferrites<sup>31</sup>, orthoferrites<sup>4</sup> and garnets<sup>6</sup>. The first uniaxial materials found to have the desired properties for bubble devices were the rare-earth orthoferrites<sup>39,48</sup>. They are of the form  $RFeO_3$ , where R is a rare-earth ion or Yttrium and are antiferromagnetic with a weak ferromagnetism caused by a slight canting (approximately  $0.5^\circ$ ) of the antiparallel spins. The molecular and magnetic unit cell is orthorhombic of sides  $a < b < c$  as shown in Fig. 2.1. The antiparallel  $Fe^{3+}$  spins align along the  $a$  axis with the  $c$  axis exhibiting the weak ferromagnetism. The sole exception is  $SmFeO_3$ , which has its net moment along the  $a$  axis at room temperature. Thus, the reorientation temperature range of  $SmFeO_3$  is  $468-487^\circ K$ , while that of the other rare-earth orthoferrites is centered around  $100^\circ K$ . The Néel temperature of all orthoferrites is approximately  $680^\circ K$ .

Orthoferrites are usually grown as single crystals by the flux method, and then sliced, polished and annealed to provide thin plates of very low coercivity ( $<0.1$  Oe). These plates are sufficiently transparent in the red to enable direct visual observation of domain behaviour by means of the longitudinal Faraday effect. Thus, domains are readily

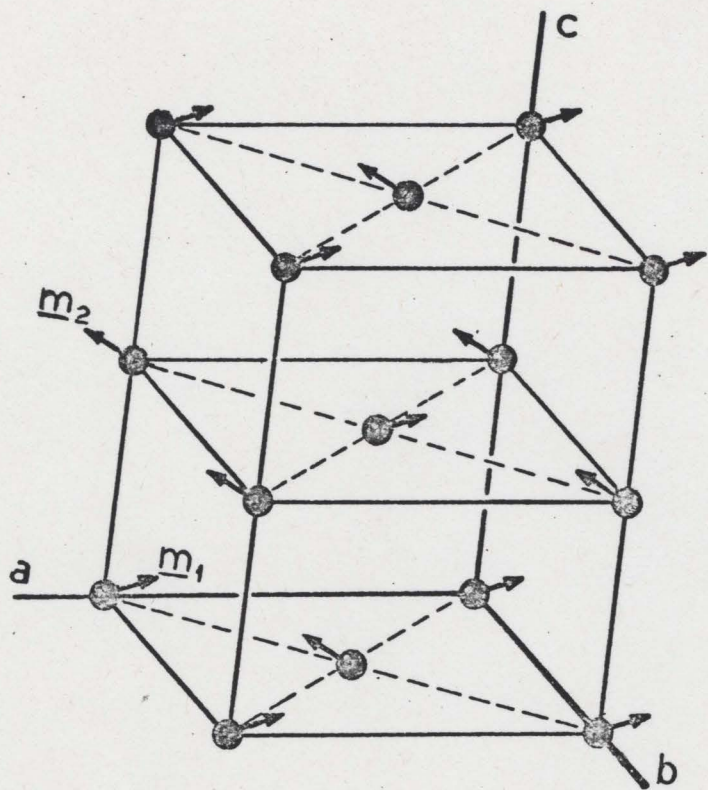


Fig. 2.1: A two-sublattice model of the spin arrangement in an orthoferrite orthorhombic cell.

visible as wavy strips when a thin plate is viewed through a polarizing microscope. The domains rotate the plane of polarization of the polarized light in opposite directions depending on their magnetic polarity. By adjusting the polarizer and analyzer on the microscope one can make half of the domains dark and the other half bright. The bubble measurements reported in this thesis were made using the Faraday effect.

If a thin orthoferrite platelet above its Néel temperature is cooled down to room temperature, spontaneously nucleated serpentine-like strip domains will be present. Such a domain pattern will usually include several single wall domains i.e., domains whose walls close upon themselves. If a prescribed bias magnetic field is then applied normal to the surface of the platelet, the single wall domains become cylindrical. As will be seen in Section 2.3, the size of the bubble domains will be governed by the bias field  $H$ , the wall energy density per unit area  $\sigma_w$ , the saturation magnetization of the material  $M_s$ , and the plate thickness  $h$ . Raising the bias field will cause the bubbles to shrink until they finally disappear at the collapse field. They are stable over roughly a 3:1 range in diameter and a 1.6:1 range in bias field.

Since a bubble domain is a localized highly stable magnetic state and can be moved about in much the same way as a charged particle, it can therefore be used to store binary information. In a practical device bubbles are normally separated by 3 or 4 domain diameters in order to minimize interaction between domains. Thus, in order to

achieve very high storage densities in devices, bubble diameters should be of the order of a few microns. Unfortunately, the single rare-earth orthoferrites provide bubble domains whose average diameters are in the range  $40\mu\text{m} - 180\mu\text{m}$ , resulting in small storage densities.

It is shown in Section 2.3 that the diameter of a stable domain is directly related to the material characteristic length  $\ell_M$  which was defined by Thiele<sup>44,45</sup> to be

$$\ell_M = \frac{\sigma_w}{4\pi M_s^2} \quad (2.1)$$

Thus, the bubble diameter can be reduced by either reducing  $\sigma_w$  or increasing  $M_s$ . Since the wall energy is proportional to the square root of the uniaxial anisotropy constant  $K_u^{12}$ , then one can decrease the bubble diameter by reducing  $K_u$ . It was mentioned above that  $\text{SmFeO}_3$  is the only rare-earth orthoferrite having an easy axis of magnetization parallel to the a axis at room temperature. It was thus reasoned by Sherwood, et al.<sup>40</sup> that a partial substitution of Sm in other rare-earth orthoferrites should result in a reduced  $K_u$ . Thus, by selecting the proper composition, the reorientation temperature range of the resulting crystal can be made to be very close to room temperature, and hence the crystal can be magnetized along both the a and c axes with comparatively weak applied (anisotropy) fields, giving a small  $K_u$ . The composition  $\text{Sm}_{0.55}\text{Tb}_{0.45}\text{FeO}_3$  for example (reorientation range:  $230-280^\circ\text{K}$ ), has a wall energy density of  $0.3 \text{ ergs/cm}^2$  (reduced from  $1.7 \text{ ergs/cm}^2$  for  $\text{TbFeO}_3$  and  $1.3 \text{ ergs/cm}^2$  for  $\text{SmFeO}_3$ ) and a material characteristic length of  $4\mu\text{m}$  at room temperature, giving bubble

diameters of the order of 20 $\mu$ m. However, as will be seen in Chapter IV,  $\sigma_w$  in the mixed rare-earth orthoferrites is sensitive to temperature fluctuations<sup>36</sup>, resulting in a large temperature sensitivity of bubble diameter.

The mixed rare-earth orthoferrites still cannot provide bubble diameters small enough to achieve packing densities of the order of 10<sup>6</sup> bits/in<sup>2</sup>. The search for new uniaxial materials has led to the discovery of the uniaxial garnets<sup>6</sup> which in general support bubbles a few microns in diameter. Furthermore, garnets are easier to grow than orthoferrites. The most promising method for making garnet bubble materials is to grow them as thin epitaxial films on nonmagnetic single-crystal substrates. Both liquid-phase<sup>38</sup> and chemical-vapor epitaxy<sup>34</sup> have been successfully used to produce garnet films. However, the saturation magnetization in garnets tends to be temperature sensitive<sup>8</sup>. Optimum plate thicknesses to minimize the temperature sensitivity of bubble diameter in garnet films are derived in Chapter IV. The condition for zero temperature sensitivity is also given.

## 2.2 Bubble Devices

The ability to combine data storage with logic at low cost in a single miniature device is the most appealing aspect of the magnetic-bubble technology. Methods of generating, shifting and detecting bubbles in devices are discussed in this section.

The simplest method of generating bubble domains in bubble devices is by cutting a bubble from a strip domain or from another

bubble<sup>4</sup>. This can be accomplished by either using a current flowing through a conductor touching the surface of the plate<sup>5</sup> (studied in Chapter V), or by utilizing the poles induced in a thin permalloy overlay circuit known as a bubble generator<sup>33</sup>, by means of an in-plane rotating field. A recent method of generation employs both a conductor and a permalloy circuit<sup>9</sup>.

Bubbles can be propagated in the magnetic medium by applying a translational force on the domains created by a gradient in  $H$ ,  $h$ ,  $\sigma_w$  or  $M_s$ <sup>47</sup>. At present, the best way of moving bubbles in devices appears to be by applying a field gradient on the domain walls, and two general methods to do this are available. The first method employs conductors in which flowing currents generate the desired field gradients<sup>5,14</sup>. This method is called conductor access. The second method, called field access, involves interacting the bubbles with permalloy overlay patterns by using either pulsating magnetic fields such as in Angelfish circuits<sup>5</sup>, or in-plane rotating fields such as in T-bar<sup>5</sup>, Y-bar<sup>15</sup> and chevron<sup>9</sup> circuits. The field access method seems more promising than the conductor access method since it is difficult to fabricate conductor patterns that have sufficient resolution to handle garnet bubbles and can carry sufficient current to move the bubbles quickly and still not vaporize. Another drawback of the conductor access method is that a great many accurately placed conductors whose dimensions are comparable to the size of the bubbles must be interconnected with external-access circuits, and any open or short-circuits in the conductor pattern would ruin the device. At present, T-bar, Y-bar and chevron patterns are almost exclusively used in bubble device

applications, since they are compatible with the bubble generator mentioned previously and have larger operating margins than Angelfish circuits. Also, bubbles can be moved in either direction in these circuits, depending on the direction of rotation of the magnetic field. The rotating fields in this case generate travelling positive and negative magnetic poles on the permalloy overlay circuits to selectively attract and repel and hence control the motion of bubbles.

Detection of bubble domains can be accomplished by one of several methods such as electromagnetic induction<sup>5</sup>, Hall effect<sup>42</sup>, direct optical sensing<sup>42</sup>, or magnetoresistance<sup>1,43</sup>. At present, the best method of detecting bubbles is using magnetoresistance, where the resistance of a permalloy film is slightly lowered in the presence of a bubble.

As mentioned earlier, bubble domains are particularly useful in applications that require logic. Several logic functions using the interaction of bubble domains in devices such as AND, OR, EXCLUSIVE OR, NAND and NOR functions have been demonstrated<sup>9,37</sup>. They are also useful in optical display applications<sup>2,13</sup>, especially where memory is desirable.

### 2.3 The Theory of Stability of Bubble Domains

In this section a brief summary of the theory of static stability of bubble domains in uniaxial platelets developed by Thiele<sup>44,45,46</sup> is presented. The results of the theory are very important in the design of bubble domain devices, since they provide conditions governing the shape, size and stability of bubbles. Some of the results will be used in subsequent chapters.

The magnetic domain structure model Thiele considered in his analysis is shown in Fig. 2.2. An isolated magnetic domain is magnetized in a platelet of effectively uniaxial low coercivity material of uniform thickness which is magnetized upward. An external magnetic field  $H$  is applied anti-parallel to the bubble magnetization. The following assumptions are made in the analysis:

1. The uniaxial platelet is of infinite extent.
2. The domain wall width is negligible in comparison to the domain radius.
3. The wall energy density per unit area is independent of either the orientation or curvature of the wall.
4. The saturation magnetization has a constant magnitude everywhere within the platelet, lying in the positive  $z$ -direction within the domain and in the negative  $z$ -direction elsewhere.
5. The domain wall is independent of  $z$ , i.e., no wall bulging occurs.
6. Domains do not spontaneously nucleate.

Thus, the bubble shape in the plane of the platelet can be described by the expansion

$$r_b(\theta) = r_0 + \Delta r_0 + \sum_{n=1}^{\infty} \Delta r_n \cos[n(\theta - \theta_n - \Delta\theta_n)] \quad (2.2)$$

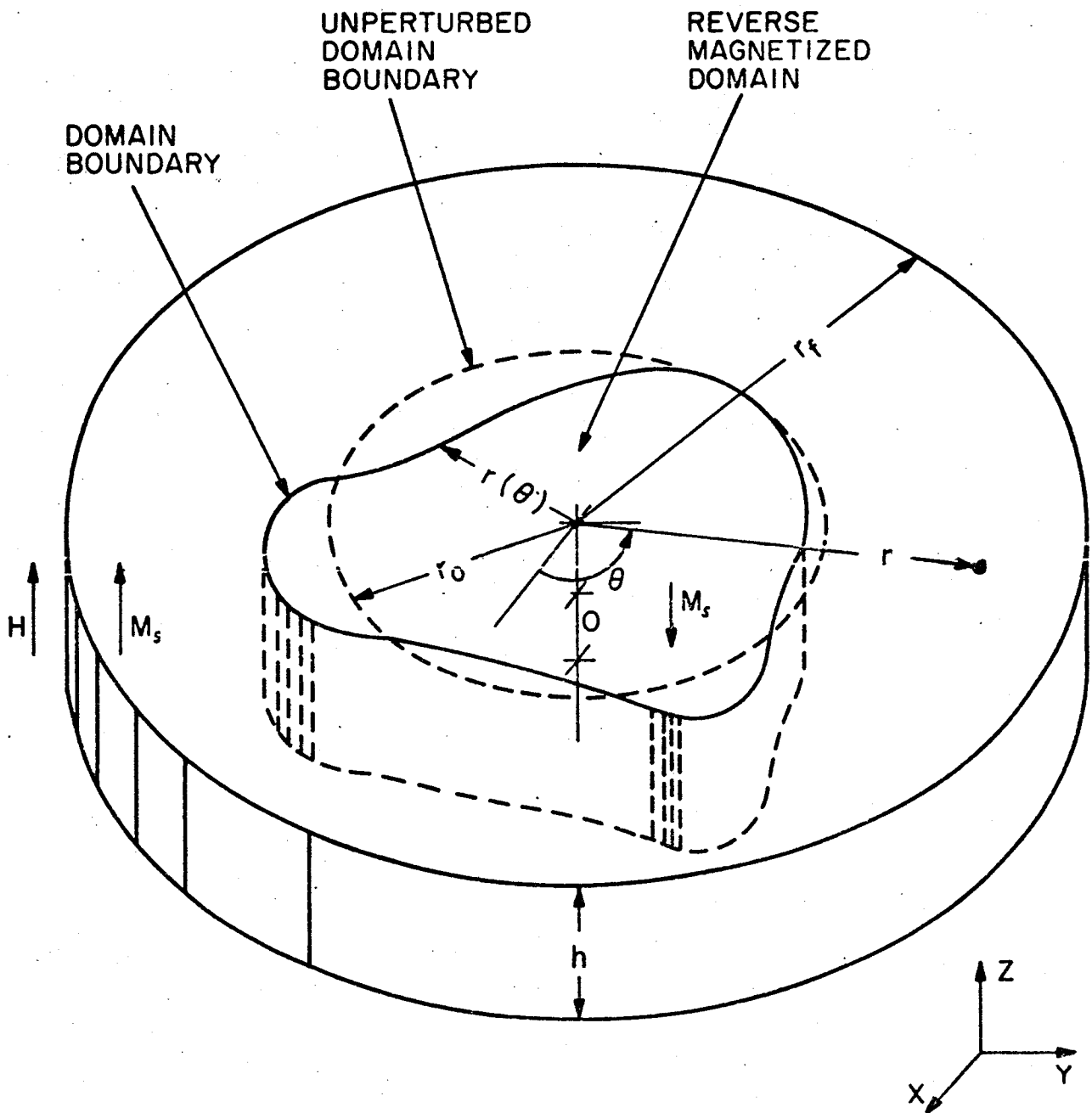


Fig. 2.2: Magnetic domain configuration and coordinate system.

where  $\Delta r_n$  and  $\Delta \theta_n$  describe small variations in domain size and shape from the circular shape of radius  $r_0$ , and

$$|r_0| \gg |\Delta r_0| + \sum_{n=1}^{\infty} n |\Delta r_n| \quad (2.3)$$

Domain size and stability can be obtained by evaluating the first and second order coefficients in the expansion of the total energy variation with respect to  $\Delta r_n$  and  $\Delta \theta_n$  about the circular domain shape given by

$$\begin{aligned} \Delta E_T = & \sum_{n=0}^{\infty} \left[ \left( \frac{\partial E_T}{\partial r_n} \right)_0 \Delta r_n + \left( \frac{\partial E_T}{\partial \theta_n} \right)_0 \Delta \theta_n \right] \\ & + \frac{1}{2} \sum_{n=0}^{\infty} \sum_{m=0}^{\infty} \left[ \left( \frac{\partial^2 E_T}{\partial r_n \partial r_m} \right)_0 \Delta r_n \Delta r_m + 2 \left( \frac{\partial^2 E_T}{\partial r_n \partial \theta_m} \right)_0 \Delta r_n \Delta \theta_m \right. \\ & \left. + \left( \frac{\partial^2 E_T}{\partial \theta_n \partial \theta_m} \right)_0 \Delta \theta_n \Delta \theta_m \right] + O_3 \end{aligned} \quad (2.4)$$

where the zero subscript indicates evaluation of the derivatives when the bubble is circular, and  $O_3$  refers to terms of order 3 and higher in the combination of  $\Delta r_n$  and  $\Delta \theta_n$ . The total energy of the domain is

$$E_T = E_W + E_H + E_M \quad (2.5)$$

where  $E_W$  is the total wall energy,  $E_H$  is the interaction energy with the externally applied field, and  $E_M$  is the internal magnetostatic energy.

With the aid of equation (2.5) one can then evaluate equation (2.4) to obtain a normalized expression for the total energy variation,

$$\begin{aligned} \frac{\Delta E_T}{2(4\pi M_s^2)(\pi h^3)} = & \left[ \frac{\ell_M}{h} + a \frac{H}{4\pi M_s} - F(a) \right] \frac{\Delta r_0}{h} + \frac{1}{2} \left\{ -\frac{2}{a} \left[ \frac{\ell_M}{h} - S_0(a) \right] \left( \frac{\Delta r_0}{h} \right)^2 \right. \\ & \left. + \sum_{n=2}^{\infty} \left( \frac{n^2-1}{a} \right) \left[ \frac{\ell_M}{h} - S_n(a) \right] \left( \frac{\Delta r_n}{h} \right)^2 \right\} + O_3 \end{aligned} \quad (2.6)$$

where  $\ell_M$  is given by equation (2.1),  $a (= \frac{2r_0}{h})$  is the aspect ratio of the domain, and  $F(a)$  and  $S_n(a)$  are the magnetostatic force and stability functions respectively and are functions of complete elliptic integrals of the first and second kind.  $F(a)$ , the radial stability function  $S_0(a)$ , and the elliptical stability function  $S_2(a)$  are plotted in Fig. 2.3.

An isolated bubble domain in an infinite uniaxial platelet will be in equilibrium when

$$\left( \frac{\partial E_T}{\partial r_0} \right)_0 = 0 \quad (2.7)$$

and stable when

$$\left( \frac{\partial^2 E_T}{\partial r_0^2} \right)_0 > 0 \quad \text{and} \quad \left( \frac{\partial^2 E_T}{\partial r_n^2} \right)_0 > 0 \quad (2.8)$$

As can be seen from equation (2.6), the equilibrium condition can be obtained by setting the coefficient of  $\frac{\Delta r_0}{h}$  equal to zero, yielding

$$\frac{\ell_M}{h} + a \frac{H}{4\pi M_s} - F(a) = 0 \quad (2.9)$$

Equation (2.9), called the force equation by Thiele<sup>44,45,46</sup>, indicates that solutions of the problem of determining the domain diameter as a function of the applied field for given values of  $\ell_M$ ,  $M_s$  and  $h$  may be obtained by graphical construction on the  $F(a)$  curve of Fig. 2.3.

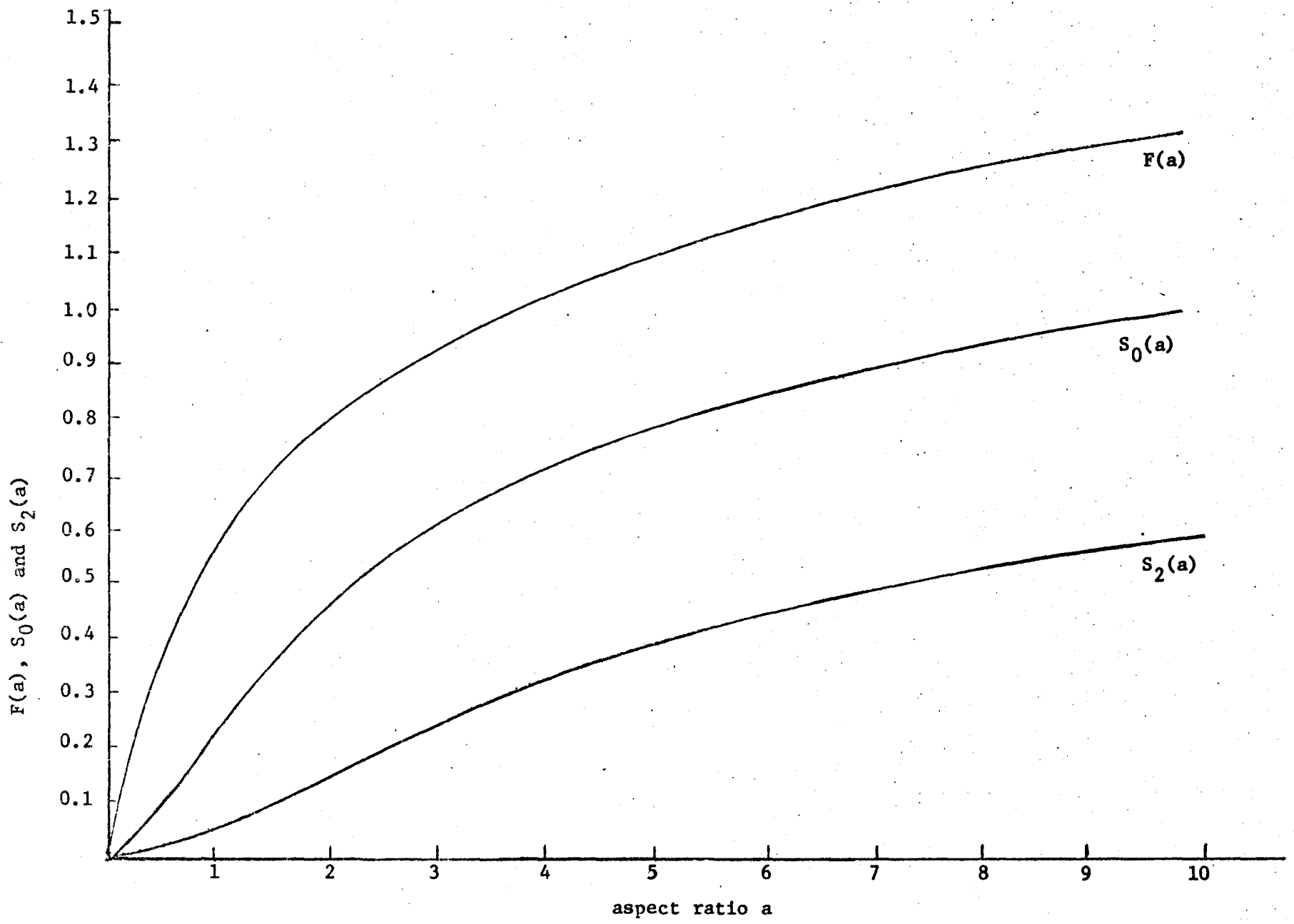


Fig. 2.3: The magnetostatic force, radial and elliptical stability functions.

The procedure consists of drawing a straight line of slope  $H/4\pi M_s$  from the point  $\ell_M/h$  on the vertical axis until it intersects  $F(a)$  at some point or points. The diameters at which these intersections occur are then solutions to the force equation. However, these solutions may be either stable or unstable. For zero or negative values of  $H$ , there is only one solution which is radially unstable. For small positive values of  $H$ , there are two solutions; the large diameter one is radially stable while the small diameter one is radially unstable. As it is increased, the diameter of the unstable solution grows, while the diameter of the stable solution decreases, until they coalesce at which the bubble domain collapses. For greater values of applied fields there are no solutions.

Since  $F(a)$  is tangential to a straight line through the origin having unit slope, the solutions will always vanish for a value of the applied field greater than  $4\pi M_s$ . Thus stable domains can exist only in the presence of a bias field having a value between zero and  $4\pi M_s$ , and a polarity tending to collapse the bubble.

The domain stability can be determined graphically by constructing a horizontal line at a height  $\ell_M/h$  in Fig. 2.3. The condition for complete stability obtained from equations (2.6) and (2.8) is

$$S_0(a) > \frac{\ell_M}{h} > S_2(a) \quad (2.10)$$

Thus,  $S_0(a)$  and  $S_2(a)$  form the boundaries of the region of stability, the former function giving the collapse condition  $d_0/h$  and the latter function the strip runout condition  $d_2/h$ .

Fig. 2.4 shows a plot of  $d_0/\ell_M$  and  $d_2/\ell_M$  as a function of  $h/\ell_M$  originally plotted by Thiele. The region between the lines is the region of total stability. Above the lines bubble domains are susceptible to elliptical perturbations and thus run out into strip domains, while below the line bubbles are radially unstable. By considering such factors as minimum bubble size and maximum stability, Thiele has obtained an optimized plate thickness given by

$$h = 4\ell_M \quad (2.11)$$

For this thickness, the center of the stable bias field range occurs at a domain diameter given by

$$d = 8\ell_M \quad (2.12)$$

In a practical device, it is also important to minimize the temperature sensitivity of bubble diameter especially since some orthoferrites and garnets have material parameters that vary strongly with temperature. Plate thicknesses that minimize temperature sensitivity of bubbles in orthoferrites and garnets are obtained in Chapter IV. A plate thickness that gives zero temperature sensitivity of bubbles in some uniaxial materials is derived in terms of the material parameters.

#### 2.4 Measurement Techniques

Characterization of bubble materials is of vital importance in the selection of the proper medium for bubble devices. Thus, several techniques for measuring relevant material parameters such as  $\ell_M$  (or

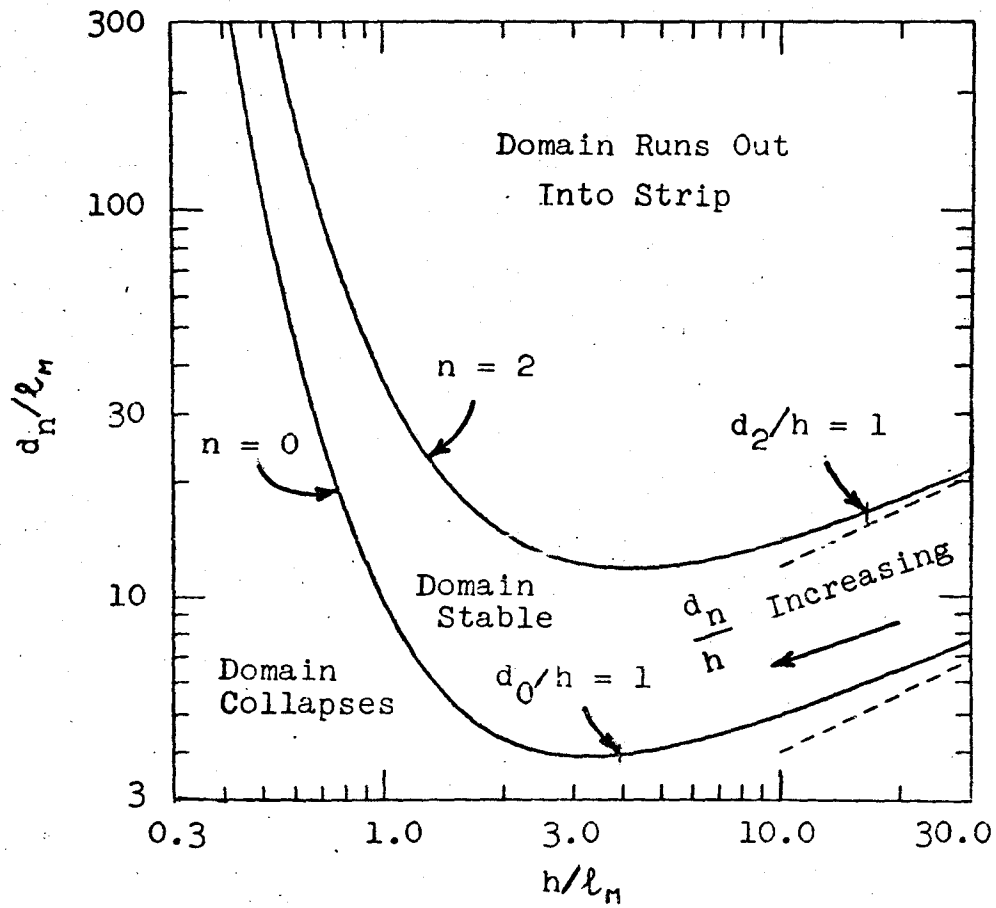


Fig. 2.4: Bubble collapse and run-out diameters as a function of plate thickness.

$\sigma_w$ ) and  $M_s$  that depend on the optical observation of domains have been developed in the last few years. Bobeck<sup>4</sup> measured both  $\ell_M$  and  $M_s$  in a material of known thickness by observing the bias field and bubble diameter at collapse. Since the collapse aspect ratio is known, then  $\ell_M/h$  can be determined from the  $S_0(a)$  curve in Fig. 2.3, and  $4\pi M_s$  can be calculated from equation (2.9). Rossol<sup>35,36</sup> measured  $\ell_M$  by measuring the stripe spacing in a demagnetized platelet and using the strip domain theory of Kooy and Enz. A method for measuring the wall energy density developed by Kurtzig and Shockley<sup>32</sup> uses a current flowing in a conductor grid of regular geometry placed under the platelet and a second array on top of the platelet and at right angles to the first. Thus, planar walls are controllably stretched into sinusoidal corrugations. The wall energy can then be obtained by calculating the external work done in increasing the wall area and subtracting from it the change in the magnetostatic energy. Although accuracies and resolutions of 5% may be obtained, this method is quite tedious. Finally, a recent method for measuring  $\ell_M$  and  $M_s$  especially useful for garnets was developed by Fowles and Copeland<sup>27</sup>. It uses both the bubble collapse method as well as the strip domain theory.

If the temperature dependence of  $\ell_M$  or  $M_s$  is required then the bubble collapse and similar methods are not practical since a new bubble has to be nucleated after each measurement. An incremental method to get around this difficulty has been developed and will be described in Chapter IV.

## 2.5 Measuring Equipment

As mentioned in Section 2.1, bubble domains in thin uniaxial plates or films can be viewed using the optical Faraday effect. The bubble measurements reported in this thesis were made using this effect. Thus, an Olympic POM polarizing microscope equipped with a built-in Bertrand lens and diaphragm was used to observe the domain behaviour. The maximum total magnification obtained from the polarizing microscope with a good resolution is 800, enabling highly precise measurements to be carried out on the single and the mixed rare-earth orthoferrites. The reticules were calibrated by means of a filar micrometer eyepiece. Since orthoferrite platelets are birefringent, a berek compensator was used to obtain maximum contrast, especially at high magnifications.

The temperature measurements reported in Chapter III were made by making use of a Leitz heating and cooling stage which fits on the microscope round stage and is capable of supplying constant sample temperatures in the range  $-35^{\circ}$  to  $350^{\circ}\text{C}$ . This made possible observing domain behaviour in  $\text{Sm}_{0.55}\text{Tb}_{0.45}\text{FeO}_3$  in the reorientation temperature region.

In order to obtain a constant bias magnetic field perpendicular to the platelet surface, a Helmholtz coil capable of producing a bias field of 80 Oe was designed to fit on the microscope stage. It was accurately calibrated by means of a Bell 640 incremental gaussmeter and an ammeter.

The cutting of strip domains described in Chapter V was carried out by means of a Chronetics PG-13A pulse generator. The current pulses were measured using a Tektronix P 6021 current probe and a Philips PM 3250 oscilloscope.

Finally, a photograph of the equipment used to observe and cut strip and bubble domains is shown in Fig. 2.5. Also shown are the strip and bubble domains as viewed in a plate of  $\text{Sm}_{0.55}\text{Tb}_{0.45}\text{FeO}_3$ .

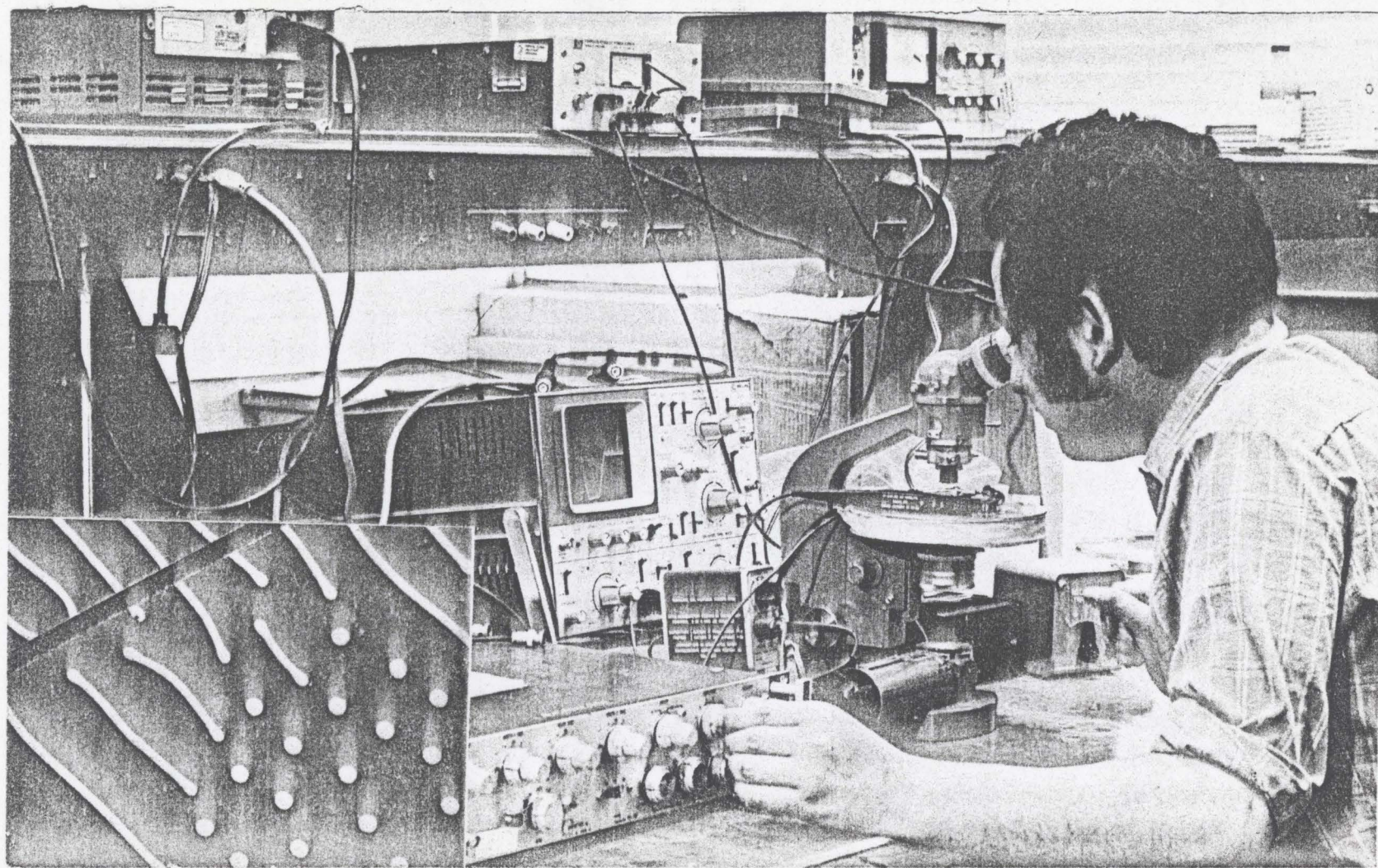


Fig. 2.5: The observation of domains in uniaxial magnetic materials.

Inset: Strip and bubble domains in a plate of  $\text{Sm}_{0.55}\text{Tb}_{0.45}\text{FeO}_3$ , as viewed using the Faraday effect (magnification x 40).

## CHAPTER III

### ANISOTROPY OF WALL ENERGY IN ORTHOFERRITES

#### 3.0 Introduction

The theory of static stability of bubble domains in uniaxial sheets was briefly discussed in Chapter II. One of the assumptions made in developing the theory is that the wall energy density is independent of wall orientation. It is shown in this chapter however, that the wall energy in orthoferrites is anisotropic, causing the otherwise circular domains to be elliptical. An experimental technique for measuring the wall-energy anisotropy based on measuring the bubble eccentricity is described and is used to measure the wall anisotropy in  $\text{Sm}_{0.55}\text{Tb}_{0.45}\text{FeO}_3$ . A study of domain walls is made by making use of a derived relationship between material parameters and wall-energy anisotropy. The study appears to verify the hypothesis that walls oriented parallel to the a axis are Bloch walls while walls oriented parallel to the b axis are Néel walls. The work described in this chapter has been reported by the author in Refs. 16, 17, 19 and 20.

#### 3.1 Wall Anisotropy

Two evidences of wall energy anisotropy in orthoferrites are elliptical domains and an apparent preferred direction for an isolated strip domain. It was shown<sup>16,17</sup> that these two effects are indeed the same, since the major axis of the elliptical domain is parallel to the preferred direction of the strip domain. This direction will be

referred to as the easy direction for the wall, not to be confused with the easy axis of magnetization which is normal to the platelet surface. The direction at right angles to the easy direction will be referred to as the hard direction. Rossol states that for  $\text{TmFeO}_3$ , the easy direction is the b crystallographic axis. As mentioned in Chapter II, the easy axis in orthoferrites at temperatures above the spin-flop temperature is the c axis, and the b axis is much harder than the a axis. It was suggested by Gyorgy and Hagedorn<sup>30</sup> that the domain walls have a continuous turning of the magnetization from the c axis through the a axis to the negative c axis independent of the wall orientation. This would imply that the walls parallel to the b axis would be Néel walls and walls parallel to the a axis would be Bloch walls. The energy of a Bloch wall<sup>12</sup> is proportional to  $\sqrt{A_b K_u}$  by either the equal angle model, where the rotation of spins is assumed to be uniform throughout the transition layers, or by the variational model which is more exact, and where the exact nature of the rotation of spins is obtained by minimizing the sum of the total exchange energy and anisotropy energy stored in the wall. The Néel wall energy<sup>30</sup> can be obtained by artificially increasing the anisotropy constant  $K_u$  by  $2\pi M_s^2$  to account for the demagnetizing fields that exist in the wall, i.e.,  $\sigma_N \propto \sqrt{A_a (K_u + 2\pi M_s^2)}$ . Thus, it is seen that

$$\frac{\sigma_B}{\sigma_N} = \sqrt{\frac{A_b/A_a}{1 + \frac{1}{q}}} \quad (3.1)$$

where

$$q = \frac{K_u}{2\pi M_s^2} \quad (3.2)$$

is the quality factor defined by Thiele<sup>44</sup>, and  $A_a$  and  $A_b$  are the exchange constants between moments separated by displacement along the a and b axis, respectively. The exchange constants are different since the atomic separation is different along the two axes<sup>48</sup>. For example, in  $TbFeO_3$ , the b side of the unit cell is 5% larger than the a side.

### 3.2 Bubble Ellipticity as a Function of Radius

The wall energy density per unit area when the wall lies along the easy axis will be denoted by  $\sigma_m$ . Rotating the wall so that it lies along the hard direction will increase the energy density by  $\sigma_x$  due to wall anisotropy. Thus, it is seen from the postulate of domain walls presented in Section 3.1 that  $\sigma_x = (\sigma_B - \sigma_N)$ . Since the magnitude of the field caused by the spins within the domain wall varies sinusoidally with the direction of the spins when the wall is between a Néel and a Bloch wall, and since  $\sigma_x$  has the form of energy per unit area, then it is seen that for an arbitrary angle  $\alpha$  between the wall direction and the hard direction, the wall energy density will be given by

$$\sigma_w = \sigma_m + \sigma_x \cos^2 \alpha \quad (3.3)$$

Fig. 3.1 shows the geometry chosen to describe the elliptical domain. Since the domains are still cylindrical, the problem can be completely described in two dimensions, and increasing the bias field causes both the bubble size and eccentricity to increase. For this configuration the total wall energy will be given by

$$E_w = h \oint \sigma_w d\ell \quad (3.4)$$

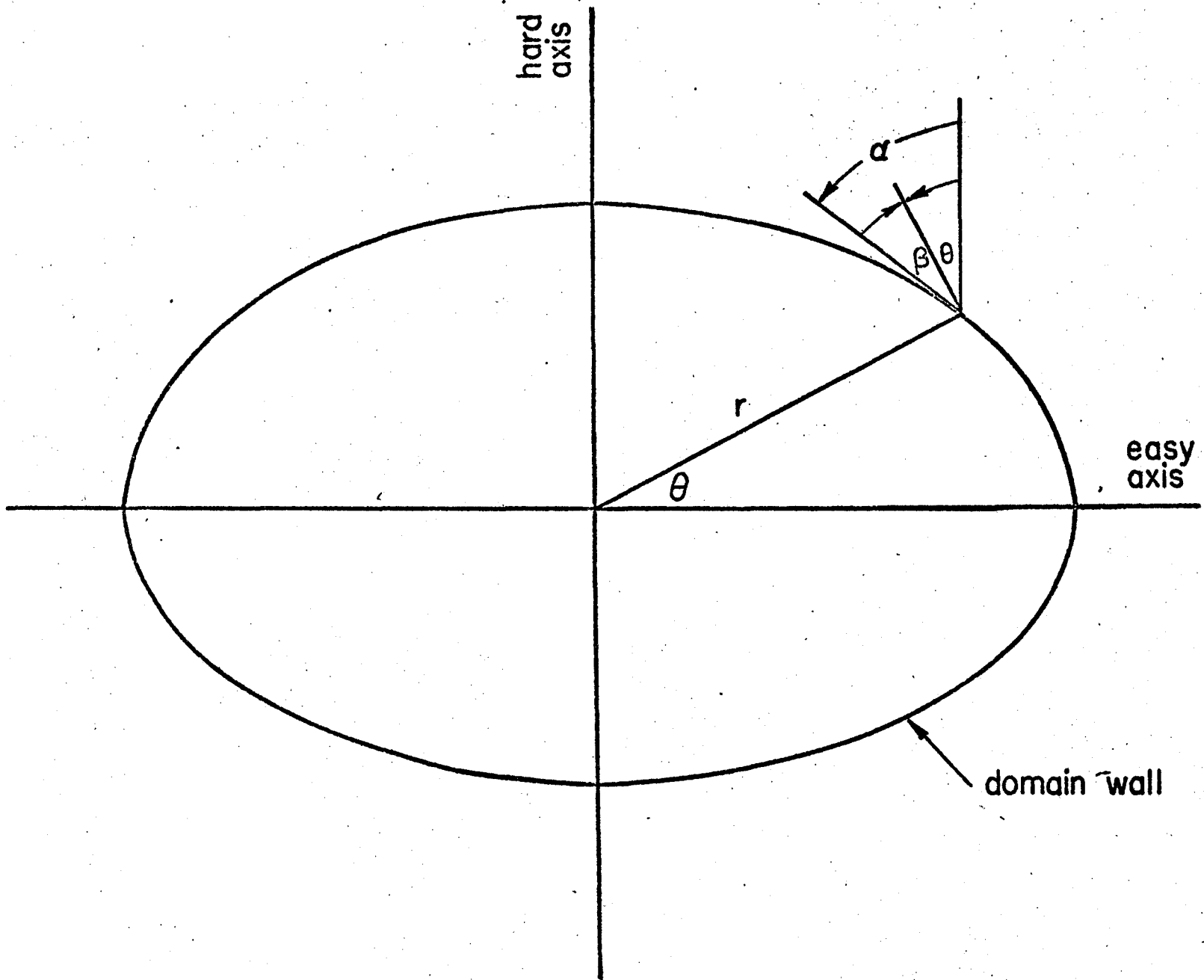


Fig. 3.1: Illustration of geometry chosen to describe an elliptical domain.

where the plate thickness  $h$  is assumed to be uniform. The integration will be carried out in terms of the polar coordinator  $\theta$ . It is seen from Fig. 3.1 that  $\alpha$  is related to  $\theta$  by

$$\theta = \alpha + \beta \quad (3.5)$$

where  $\beta$  is the angle between the tangent line and the normal to the radius vector at a point on the curve; and since angles are taken to be positive in the counter-clockwise sense,  $\beta$  is negative as shown in Fig. 3.1. For small deviations from a circle,  $\beta$  is given by

$$\beta \approx \sin \beta \approx \frac{dr/d\theta}{r}, \quad \cos \beta \approx 1 \quad (3.6)$$

In order to use the results of Thiele, the perturbation from a circular domain shall be assumed to take the form

$$r = r_0 + r_2 \cos 2\theta \quad (3.7)$$

where  $r_2$  is a second-order variation from a circle. Then from equation (3.5),

$$\cos \alpha = \cos \theta \cos \beta + \sin \theta \sin \beta \quad (3.8)$$

and from equation (3.6)

$$\cos^2 \alpha = \cos^2 \theta + \frac{1}{r} \frac{dr}{d\theta} \sin^2 \theta + \left(\frac{1}{r} \frac{dr}{d\theta}\right)^2 \sin^2 \theta \quad (3.9)$$

Substituting equation (3.7) into equation (3.9), eliminating terms of order  $r_2^2$  and higher order, assuming small perturbation, and using equation (3.3) yields,

$$\sigma_w = \sigma_m + \sigma_x \left( \cos^2 \theta - \frac{2r_2}{r_0} \sin^2 2\theta \right) \quad (3.10)$$

To the first order in  $r_2$ ,  $d\ell$  is given by

$$d\ell = (r_0 + r_2 \cos 2\theta)d\theta \quad (3.11)$$

Therefore, from equation (3.4),

$$E_w = h \int_0^{2\pi} [r_0 \sigma_m + r_0 \sigma_x \cos^2 \theta - 2\sigma_x r_2 \sin^2 2\theta + r_2 \sigma_m \cos 2\theta + r_2 \sigma_x \cos^2 \theta \cos 2\theta] d\theta \quad (3.12)$$

or

$$E_w = \pi h [r_0 (2\sigma_m + \sigma_x) - \frac{3\sigma_x r_2}{2}]$$

This shows that the wall energy will be decreased by increasing  $r_2$ .

This is the same result obtained by Della Torre<sup>18</sup> using more general

methods. It can be seen from equation (2.6) that for the case  $\sigma_x=0$ ,

the change in energy from the circular case  $r_2=0$  using the perturbation

described by equation (3.1) is given by

$$\Delta E = \pi r_2^2 = \frac{3(\pi h^3) 4\pi M_s^2}{2r_0 h} \left[ \frac{\ell_M}{h} - S_2(a) \right] r_2^2 \quad (3.14)$$

where in this case the material characteristic length is defined as

$$\ell_M = \frac{\sigma_a}{4\pi M_s^2} \quad (3.15)$$

$\sigma_a$  is the average wall energy density given by

$$\sigma_a = \sigma_m + \frac{\sigma_x}{2} = \frac{1}{2}(\sigma_B + \sigma_N) \quad (3.16)$$

The equilibrium value of  $r_2$  may be obtained by minimizing the total energy,

i.e., the sum of equations (3.13) and (3.14) with respect to  $r_2$ .

Differentiating this sum and setting it equal to zero yields

$$r_2 = \frac{3\pi h \sigma_x}{4k} \quad (3.17)$$

Since this result can be used as an experimental technique for measuring  $\sigma_x$ , it is more convenient to solve equation (3.17) for  $\sigma_x$

$$\sigma_x = 2h(4\pi M_s^2) \left[ \frac{\ell_M}{h} - S_2(a) \right] \frac{r_2}{r_0} \quad (3.18)$$

or

$$\sigma_x / \sigma_a = \left[ 1 - \frac{h S_2(a)}{\ell_M} \right] \frac{e^2}{2} \quad (3.19)$$

where  $e (\approx 2\sqrt{r_2/r_0})$  is the eccentricity of the ellipse<sup>11</sup> for small values of  $r_2/r_0$ .

### 3.3 Experimental Methods and Results

Measurements of the eccentricity as a function of the average radius of an isolated bubble domain were carried out on several samples of  $\text{Sm}_{0.55}\text{Tb}_{0.45}\text{FeO}_3$ . Results of a typical run are shown in Fig. 3.2. These measurements were carried out on a 61- $\mu\text{m}$  thick plate of  $\text{Sm}_{0.55}\text{Tb}_{0.45}\text{FeO}_3$  at 25°C. For this material,  $\ell_M = 3.6\mu\text{m}$  and  $4\pi M_s = 106$  EMU. The solid line is the best fit using equation (3.17). Microscope resolution limited reliable results to bubble radii greater than twice the collapse radius  $r_c$ . It is noted that  $e$  approaches infinity for  $r_0 \approx 2.8 r_c$ , corresponding to bubble strip transition. It is also noted that the curves do not extrapolate to  $e=0$  as  $r \rightarrow 0$ , but

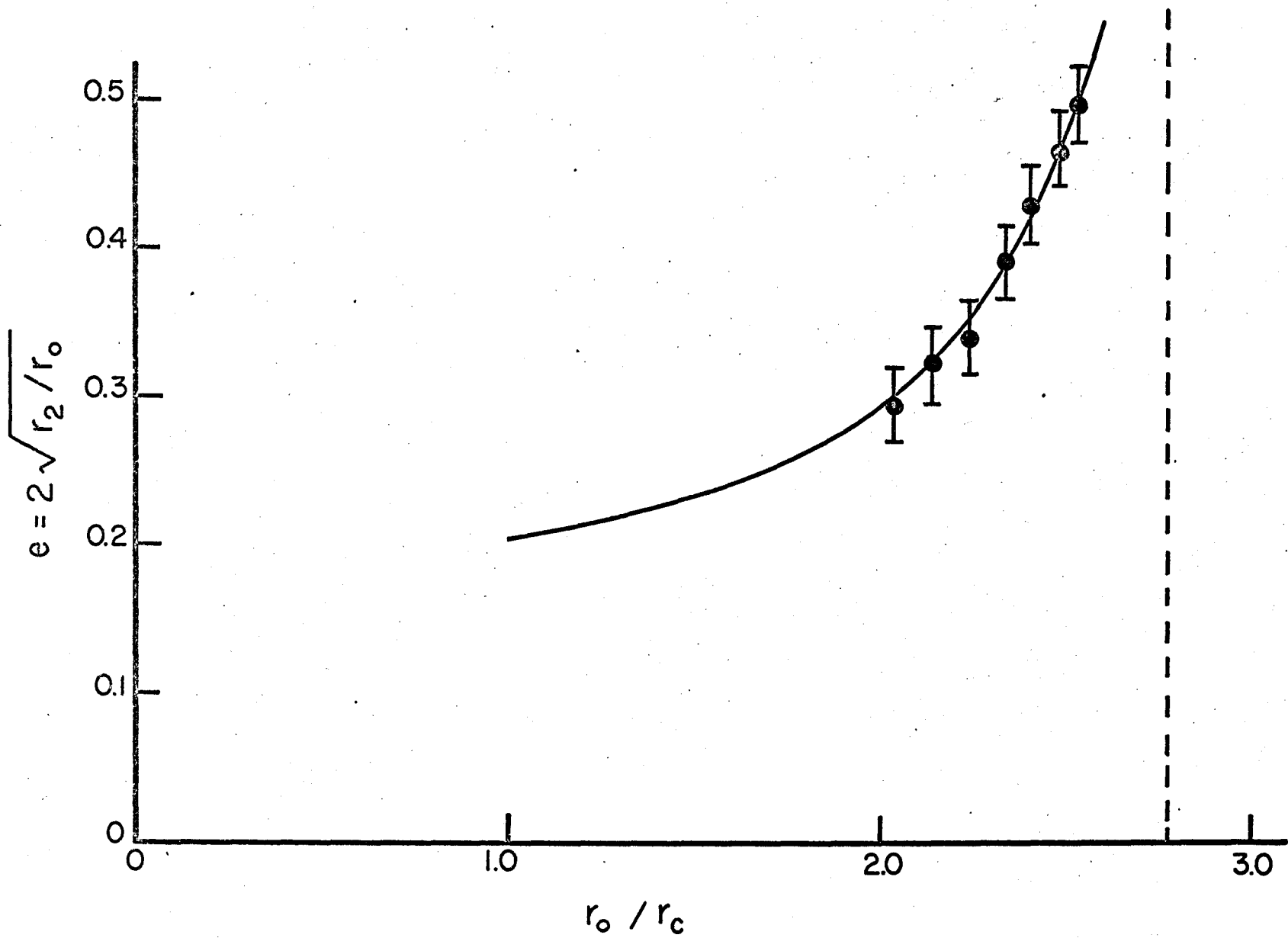


Fig. 3.2: Eccentricity of the elliptical domain as a function of bubble radius.

rather to  $e=0.18$ .

In order to obtain a determination of  $\sigma_x$ , equation (3.19) was used to replot these results, as is shown in Fig. 3.3. It is noted that all the measurements yielded essentially the same value for  $\sigma_x/\sigma_a$  of 0.017, or  $\sigma_x = 0.0055$  ergs/cm<sup>2</sup>.

The above measurements indicate that the Bloch wall has a 1.7% greater wall energy than the Néel wall in  $\text{Sm}_{0.55}\text{Tb}_{0.45}\text{FeO}_3$ . However, from known data the term  $\sqrt{1 + \frac{1}{q}}$  would imply that the Néel wall has a 1.8% greater wall energy since  $q \approx 28$ . Therefore, in the absence of other effects, one would expect that  $A_b \approx 1.07 A_a$ .

In order to verify the hypothesis that domain walls parallel to the a-axis are Bloch walls while walls parallel to the b axis are Néel walls, a sample of  $\text{Sm}_{0.55}\text{Tb}_{0.45}\text{FeO}_3$  was subjected to a temperature test. At room temperature, the  $q$  of the material is approximately 25 due to the proximity of the spin-flop temperature.<sup>28</sup> As the temperature of the sample is raised the value of  $q$  increases approaching, for high temperatures, that of a single rare-earth orthoferrite. Neglecting any change in  $A_b/A_a$  with temperature due to the low thermal expansion coefficient of orthoferrites,<sup>29</sup> one can then test equation (3.1) and hence the hypothesis by varying  $q$  indirectly by changing the temperature of the sample.

The  $q$  of the sample was measured on a vibrating sample magnetometer as a function of temperature using the method described by Sherwood et al.<sup>40</sup> A typical measurement at 23°C of the magnetization as a function of field applied parallel to the a and b axes is shown in Fig. 3.4 (curves (a) and (b), respectively). Curve (c) is obtained by

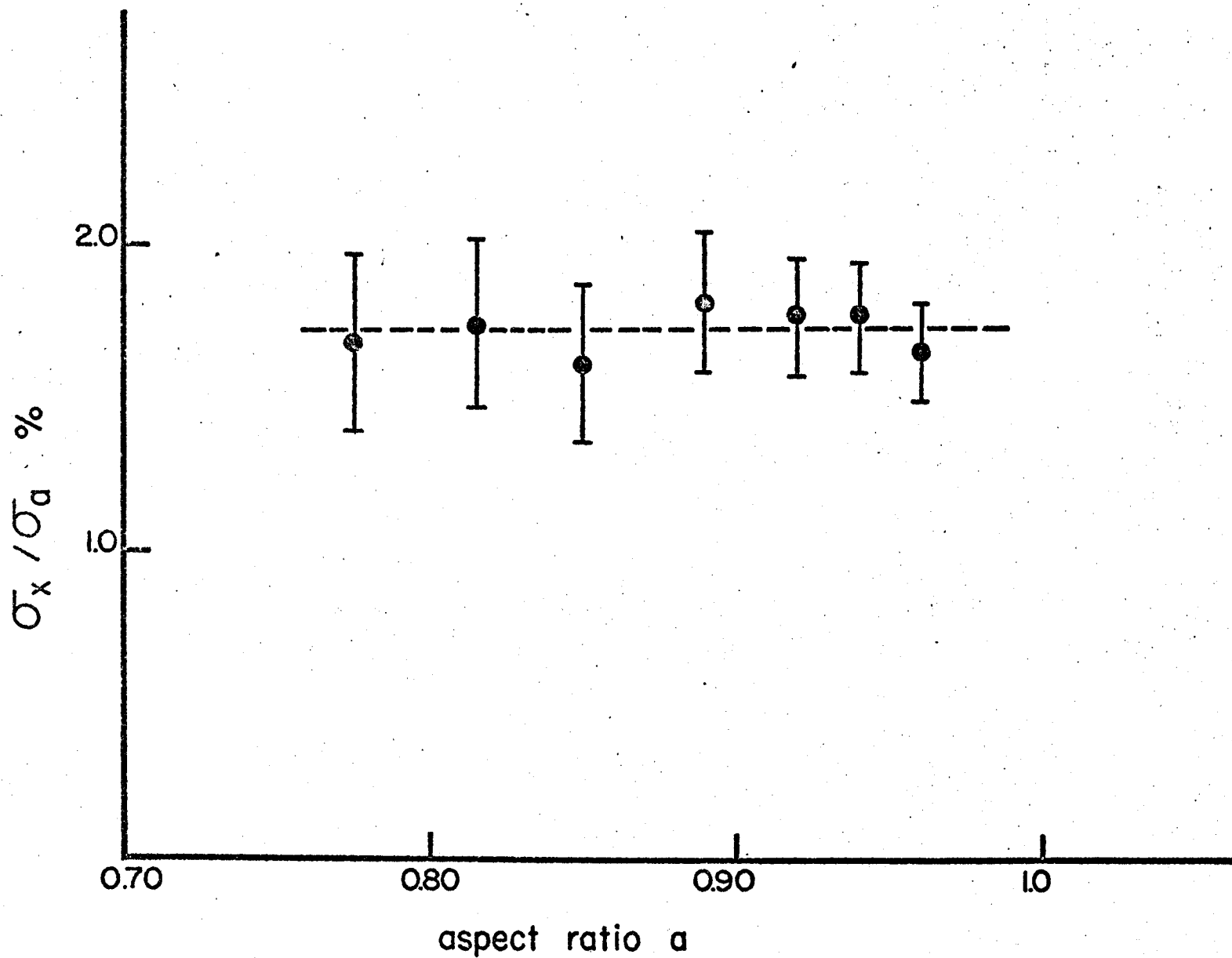


Fig. 3.3: Measurements of wall energy anisotropy as a function of domain aspect ratio.

subtracting (b) from (a). The anisotropy field  $H_a$  can be determined from the intersection of the low- and high-field asymptotes of (c). It should be pointed out that an approximately 20% fourth-order anisotropy results in a 6% increase in both the Bloch and Néel wall energies, but does not affect the values of  $H_a$  appreciably. Thus, it is possible to test equation (3.1) for  $q$  varying between approximately 25 and 85 (obtained at 70°C) using this technique as shown in Fig. 3.5. For higher temperatures where the anisotropy field is greater than 7 kOe, it becomes increasingly difficult to obtain accurate values of  $q$  from the magnetization curves. Since the maximum magnetic field supplied by the electromagnet is limited to 14 kOe, it is not possible to define the high-field asymptote properly at higher temperatures. It might also be added that as the temperature of the sample approaches the spin flop temperature,  $q$  decreases towards zero. Thiele<sup>44</sup> claimed that for device operation  $q$  should probably be greater than two. It was observed, however, that in order to obtain reasonably well-defined bubbles in orthoferrites,  $q$  should be at least of the order of 10.

Thus, equation (3.1) can be tested by using equation (3.19),

$$\frac{\sigma_x}{\sigma_a} = 2 \frac{\sigma_B/\sigma_N - 1}{\sigma_B/\sigma_N + 1} = \left[ 1 - \frac{hS_2(a)}{\ell_M} \right] \frac{e^2}{2} \quad (3.19)$$

Of these parameters,  $\ell_M$  is the only one that cannot be observed directly. Two methods can be used to determine the temperature dependence of  $\ell_M$ . The domain collapse method described in Chapter II and used by Rossol<sup>36</sup> in his temperature measurements requires the nucleation of a new bubble after each measurement. The second method, used here and described in

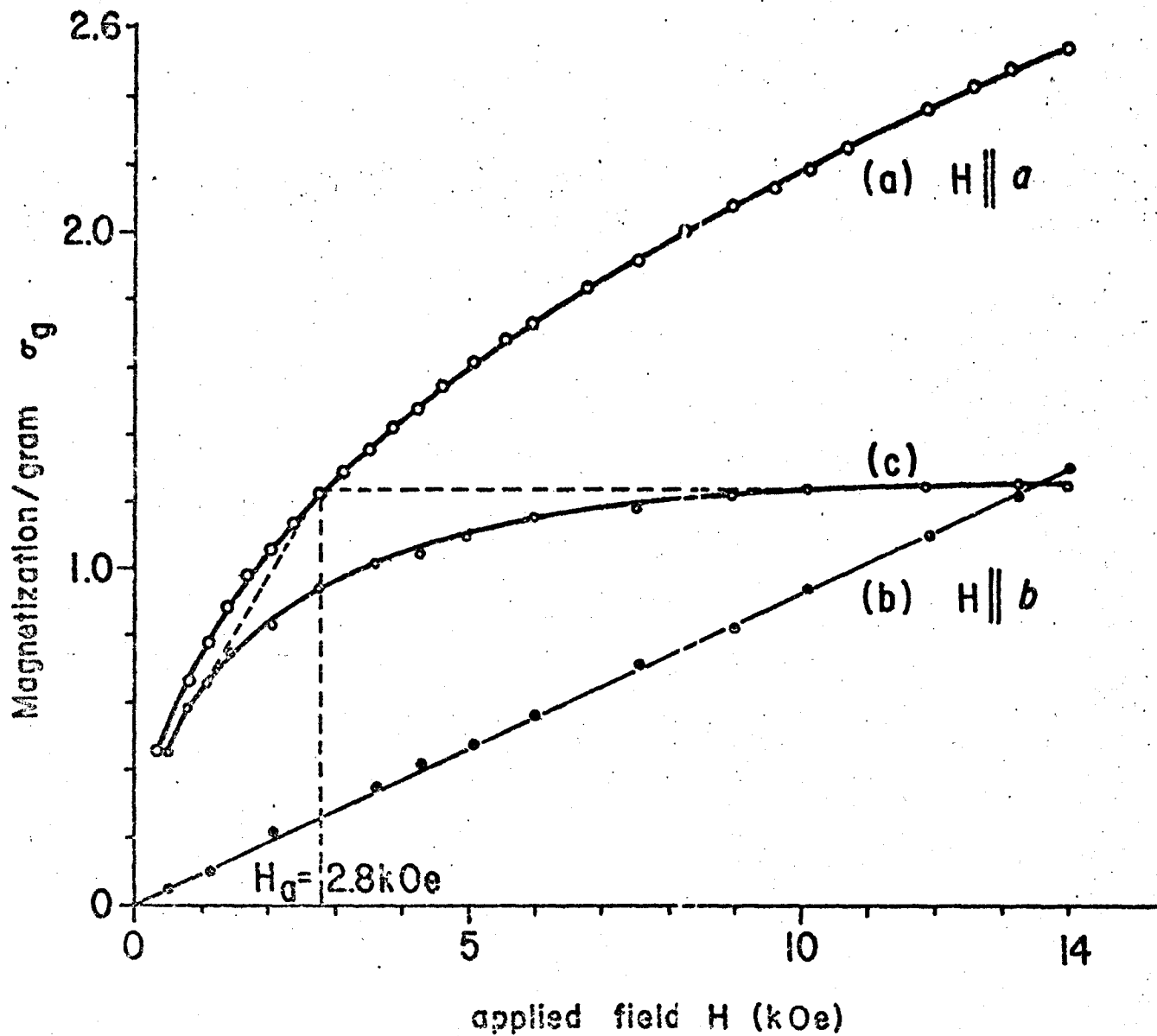


Fig. 3.4: Illustration of technique for measuring the anisotropy field at room temperature using curves of magnetization versus field.

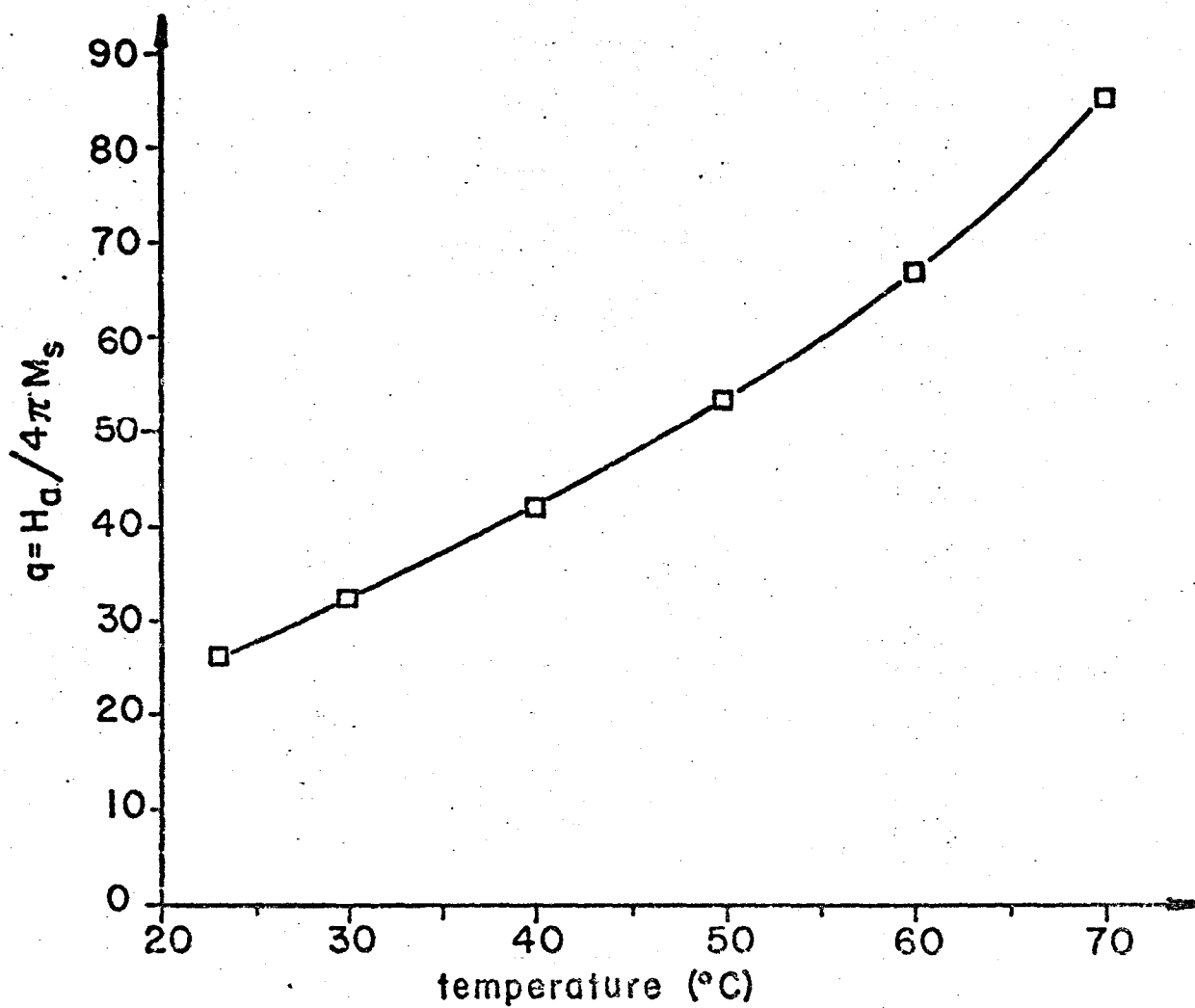


Fig. 3.5: The quality factor as a function of temperature obtained from vibrating sample magnetometer measurements.

detail in Chapter IV, requires observing the change in radius  $\Delta r_0$  of an isolated magnetic domain when the temperature of the sample is varied and the bias magnetic field remains fixed without destroying the bubble. This method can also predict the temperature variation of  $q$ .

Measurements of  $\sigma_x/\sigma_a$  as a function of temperature were carried out on a 60- $\mu\text{m}$  thick plate of  $\text{Sm}_{0.55}\text{Tb}_{0.45}\text{FeO}_3$  and the results are shown in Fig. 3.6. The solid line represents the average values of  $\sigma_x/\sigma_a$  obtained by measuring the bubble eccentricity as a function of mean domain radius at a particular temperature and then using equation (3.19). It might have been noted from equation (3.1) that at high temperatures where  $q$  is large,  $\sigma_B/\sigma_N$  approaches  $\sqrt{A_b/A_a}$ . High temperature extrapolation of  $\sigma_x/\sigma_a$  shows that  $A_b/A_a \approx 1.076$ , which agrees well with measurements made at room temperature and given above. Using this value of  $A_b/A_a$  and the values of  $q$  as a function of temperature obtained from vibrating sample magnetometer measurements,  $\sigma_x/\sigma_a$  was calculated and represented on Fig. 3.6 by circles. On the other hand, using values of  $q$  obtained from the method described in Chapter IV, the  $\sigma_x/\sigma_a$  values are represented in Fig. 3.6 by triangles.

Thus, measurements of the wall-energy anisotropy in orthoferrites seem to verify its predicted dependence on  $q$ . This appears to be an indication of the validity of the hypothesis that walls oriented parallel to the axis are Bloch walls, while walls oriented parallel to the  $b$  axis are Néel walls.

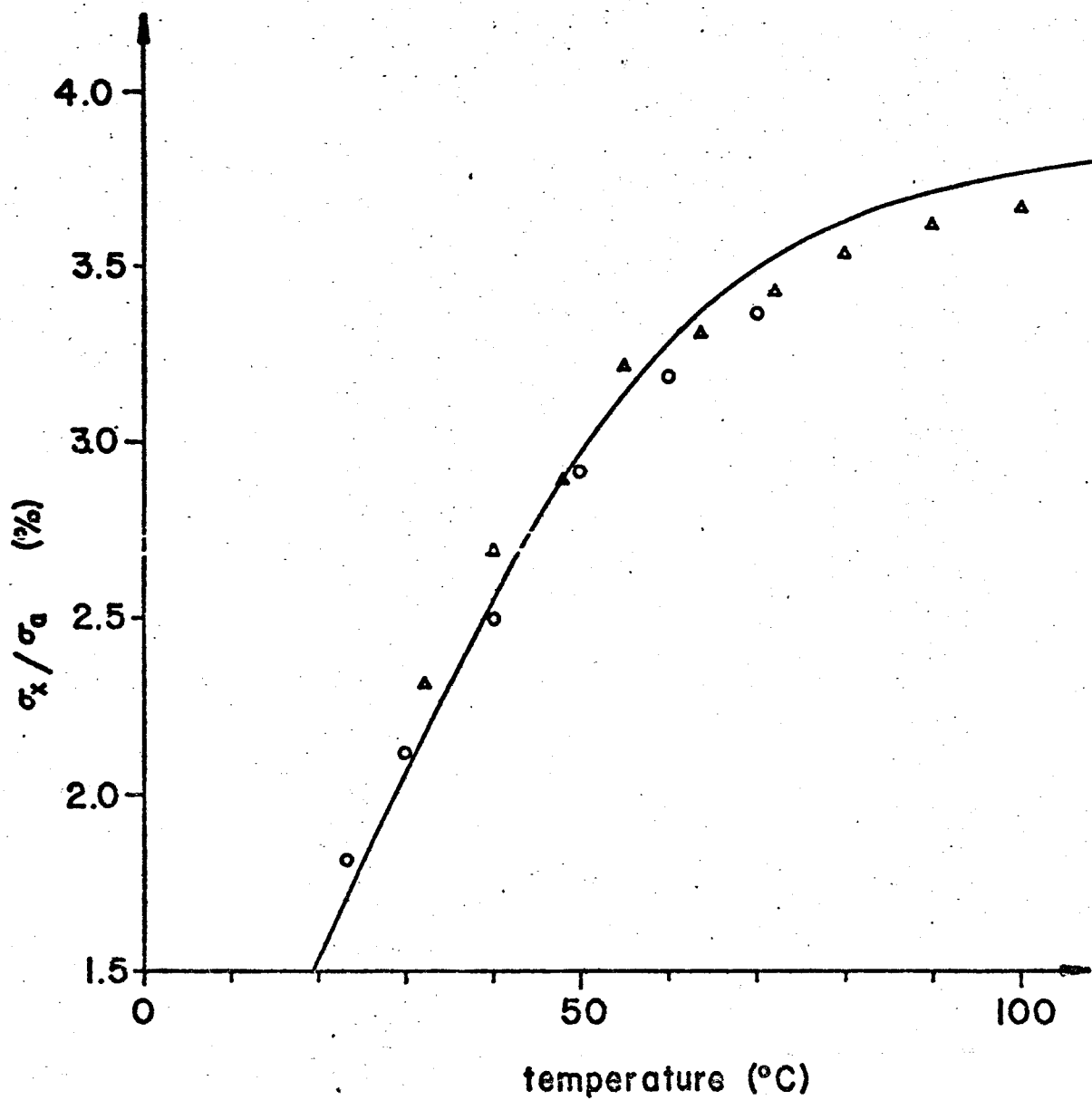


Fig. 3.6: Measurements of  $\sigma_x / \sigma_a$  as a function of the temperature of the sample.

### 3.4 Conclusions

A method for measuring the wall energy anisotropy in orthoferrites, which causes bubble domains to be elliptical, has been described and used to measure the wall anisotropy in  $\text{Sm}_{0.55}\text{Tb}_{0.45}\text{FeO}_3$ . Measurements of the wall-energy anisotropy as a function of quality factor of the material seem to verify the hypothesis that, in orthoferrites, walls parallel to the a axis are Bloch walls while walls parallel to the b axis are Néel walls.

## CHAPTER IV

### TEMPERATURE SENSITIVITY OF BUBBLE DOMAINS

#### 4.0 Introduction

Several techniques for measuring the wall energy density and the saturation magnetization in uniaxial materials have been discussed in Chapter II. In this chapter, a method suitable for measuring the temperature dependence of  $\sigma_w$  in the mixed rare-earth orthoferrites<sup>19,20</sup>, and  $M_s$  in some uniaxial garnets<sup>2</sup> are described. The advantage of the method is that it uses an isolated bubble domain without the need to destroy the bubble in order to obtain the measurements.

As discussed in Chapter II, Thiele obtained an optimum material thickness for bubble device applications by considering such factors as smallest bubble size and optimum bubble stability. In a practical device, it is desirable to minimize its temperature dependence. Thus, optimum plate thicknesses to minimize the variation of bubble diameter with temperature in both orthoferrites and garnets are considered<sup>22</sup>. Also, the condition for zero temperature sensitivity of bubble domains in some uniaxial materials is obtained in terms of the material parameters<sup>25</sup>. This work has been reported by the author in Refs. 19, 20, 21, 22 and 25.

#### 4.1 A Method for Measuring the Temperature Dependence of $\sigma_w$ and $q$ in the Mixed Rare-Earth Orthoferrites

In the mixed rare-earth orthoferrites the wall energy densities vary strongly with temperature at temperatures in the vicinity of the

reorientation region<sup>36</sup> which yield smallest bubble sizes, while the magnetizations are almost constant.

From equation (2.9), the force equation for an isolated bubble domain in an infinite uniaxial plate is given by

$$\frac{\ell_M}{h} + a \frac{H}{4\pi M_s} - F(a) = 0 \quad (2.9)$$

Substituting for  $\ell_M$  and  $a$  yields

$$\frac{\sigma_w}{4\pi M_s^2 h} + \frac{d}{h} \frac{H}{4\pi M_s} - F\left(\frac{d}{h}\right) = 0 \quad (4.1)$$

If the temperature of the sample is raised by say,  $\Delta t$ , one would expect  $\sigma_w$  to increase by an amount  $\Delta\sigma_w$ , while the bubble diameter will decrease by  $\Delta d$  for a fixed bias field. Neglecting any change in  $M_s$ , the force equation thus becomes

$$\frac{\sigma_w + \Delta\sigma_w}{4\pi M_s^2 h} + \left(\frac{d - \Delta d}{h}\right) \frac{H}{4\pi M_s} - F\left(\frac{d - \Delta d}{h}\right) = 0 \quad (4.2)$$

Subtracting equation (4.2) from equation (4.1) gives

$$-\frac{\Delta\sigma_w}{4\pi M_s^2 h} + \frac{\Delta d}{h} \frac{H}{4\pi M_s} + F\left(\frac{d - \Delta d}{h}\right) - F\left(\frac{d}{h}\right) = 0 \quad (4.3)$$

Expanding  $F\left(\frac{d - \Delta d}{h}\right)$  in a Taylor series and neglecting second and higher order terms in  $\Delta d$ , one obtains

$$F\left(\frac{d - \Delta d}{h}\right) \approx F\left(\frac{d}{h}\right) - \Delta d \frac{\partial F(d/h)}{\partial d} \quad (4.4)$$

Also, from Thiele<sup>44</sup>,

$$\frac{\partial F(d/h)}{\partial d} = \frac{1}{d} [F(d/h) - S_0(d/h)] \quad (4.5)$$

Therefore, substituting equations (4.4) and (4.5) in equation (4.3) yields

$$-\frac{\Delta\sigma_w}{4\pi M_s^2 h} + [F(a) - \frac{\ell_M}{h}] \frac{\Delta d}{d} - [F(a) - S_0(a)] \frac{\Delta d}{d} \approx 0 \quad (4.6)$$

or

$$\frac{\Delta\sigma_w}{\sigma_w} \approx \left( \frac{hS_0(a)}{\ell_M} - 1 \right) \frac{\Delta d}{d} \quad (4.7)$$

Also, since<sup>44</sup>  $\sigma_w = 4M_s \sqrt{2\pi Aq}$ , and neglecting the change in A and  $M_s$  for temperatures well below the Néel temperature, it follows that  $\sigma_w$  is proportional to  $\sqrt{q}$ . Therefore, it is seen that

$$\frac{\Delta\sigma_w}{\sigma_w} = \frac{\Delta q}{2q} \approx \left[ \frac{hS_0(a)}{\ell_M} - 1 \right] \frac{\Delta d}{d} \quad (4.8)$$

Thus, by starting with the known values of  $\sigma_w$  (obtained from the domain collapse method described in Chapter II) and  $q$  (obtained from vibrating sample magnetometer measurements as shown in Chapter III), one can then proceed to obtain the incremental changes  $\Delta\sigma_w$  and  $\Delta q$  by using equation (4.8). If this is done at fixed temperature intervals, it would then be possible to determine the temperature dependence of  $\sigma_w$  and  $q$  without collapsing the original domain. This method was used in measuring the temperature dependence of the wall-energy anisotropy in  $\text{Sm}_{0.55}\text{Tb}_{0.45}\text{FeO}_3$  as described in Chapter III.

#### 4.2 A Method for Measuring the Temperature Dependence of $M_s$ in Uniaxial Garnets

In general, the uniaxial garnets at room temperature have magnetizations which are strong functions of temperature due to the proximity of the compensation point<sup>8</sup>. On the other hand, the wall energy densities vary little with temperature in most garnets. Thus a similar method to the one described in Section 4.1 can be used to measure the temperature dependence of the magnetization for such materials.

If the temperature of the sample is say lowered by a small amount, then the magnetization of the mean bubble diameter will decrease by  $\Delta M_s$  and  $\Delta d$ , respectively, for a fixed bias field. In this case, the force equation given by equation (4.1) becomes

$$\frac{\sigma_w}{4\pi(M_s - \Delta M_s)^2 h} + \frac{(d - \Delta d)}{h} \frac{H}{4\pi(M_s - \Delta M_s)} - F\left(\frac{(d - \Delta d)}{h}\right) = 0 \quad (4.9)$$

Neglecting second and higher order terms in  $\Delta M_s/M_s$  gives

$$\frac{\sigma_w}{4\pi M_s^2 h} \left(1 + \frac{2\Delta M_s}{M_s}\right) + \frac{(d - \Delta d)}{h} \frac{H}{4\pi M_s} \left(1 + \frac{\Delta M_s}{M_s}\right) - F\left(\frac{(d - \Delta d)}{h}\right) = 0 \quad (4.10)$$

Subtracting equation (4.10) from equation (4.1) and again neglecting second and higher order terms,

$$-\frac{\sigma_w}{4\pi M_s^2 h} \frac{2\Delta M_s}{M_s} + \left(\frac{\Delta d}{h} - \frac{d}{h} \frac{H}{4\pi M_s}\right) \frac{H}{4\pi M_s} + F\left(\frac{(d - \Delta d)}{h}\right) - F\left(\frac{d}{h}\right) \approx 0 \quad (4.11)$$

Using equations (2.1), (4.4) and (4.5) equation (4.11) becomes

$$-\frac{2\Delta M_s}{M_s} \frac{\ell_M}{h} + (F(a) - \frac{\ell_M}{h}) \left( \frac{\Delta d}{d} - \frac{\Delta M_s}{M_s} \right) - \frac{\Delta d}{d} [F(a) - S_0(a)] \approx 0 \quad (4.12)$$

or

$$\frac{\Delta M_s}{M_s} \approx \frac{(S_0(a) - \ell_M/h) \frac{\Delta d}{d}}{F(a) + \ell_M/h} \quad (4.13)$$

Therefore, in a similar manner to the method described in section 4.1, one can start with the known value of the magnetization of the garnet (obtained from domain collapse or magnetometer measurements) and then proceed to measure the incremental changes  $\Delta M_s$  by using equation (4.13). Doing this at fixed temperature intervals would give the temperature dependence of  $M_s$  without collapsing the original bubble.

#### 4.3 Temperature Sensitivity of Bubble Domains

The temperature sensitivity of bubble diameter,  $S$ , is defined

by

$$S \triangleq \frac{1}{d} \frac{\Delta d}{\Delta T} \quad (4.14)$$

where  $\Delta T$  is the change in temperature. For materials whose temperature dependence is predominantly due to wall energy variation such as orthoferrites and especially the mixed rare-earth orthoferrites, this may be written as

$$S_0 = \frac{\rho_0}{\sigma_w} \frac{\Delta \sigma_w}{\Delta T} \quad (4.15)$$

where

$$\rho_0 = \frac{\sigma_w}{\Delta \sigma_w} \frac{\Delta d}{d} \quad (4.16)$$

Using equation (4.7), equation (4.16) becomes

$$\rho_0 = \frac{\ell_M/h}{S_0(a) - \ell_M/h} \quad (4.17)$$

For materials whose temperature dependence is predominantly due to magnetization variation such as some of the uniaxial garnets, the sensitivity may be written as

$$S_g = \frac{\rho_g}{M_s} \frac{\Delta M_s}{\Delta T} \quad (4.18)$$

where

$$\rho_g = \frac{M_s}{d} \frac{\Delta d}{\Delta M_s} \quad (4.19)$$

Substituting equation (4.13) in equation (4.19) yields

$$\rho_g = \frac{F(a) + \ell_M/h}{S_0(a) - \ell_M/h} \quad (4.20)$$

It may be noted that

$$\rho_g = \frac{F(a)}{S_0(a) - \ell_M/h} + \rho_0 \quad (4.21)$$

where the two functions satisfy  $F(a) > 0$  and  $S_0(a) > \frac{\ell_M}{h}$ . Consequently,

$$\rho_g > \rho_0 \quad (4.22)$$

Values of  $\rho_0$  and  $\rho_g$  are plotted in Fig. 4.1 as a function of plate thickness. Two bias conditions for bubble diameters were used: the geometric mean diameter  $\sqrt{d_0 d_2}$  and the arithmetic mean diameter  $\frac{1}{2}(d_0 + d_2)$ , where  $d_0$  is the bubble collapse diameter and  $d_2$  is the run-out diameter. It is seen from Fig. 4.1 that a smaller temperature sensitivity is obtained if one uses the arithmetic mean diameter as the bias condition.

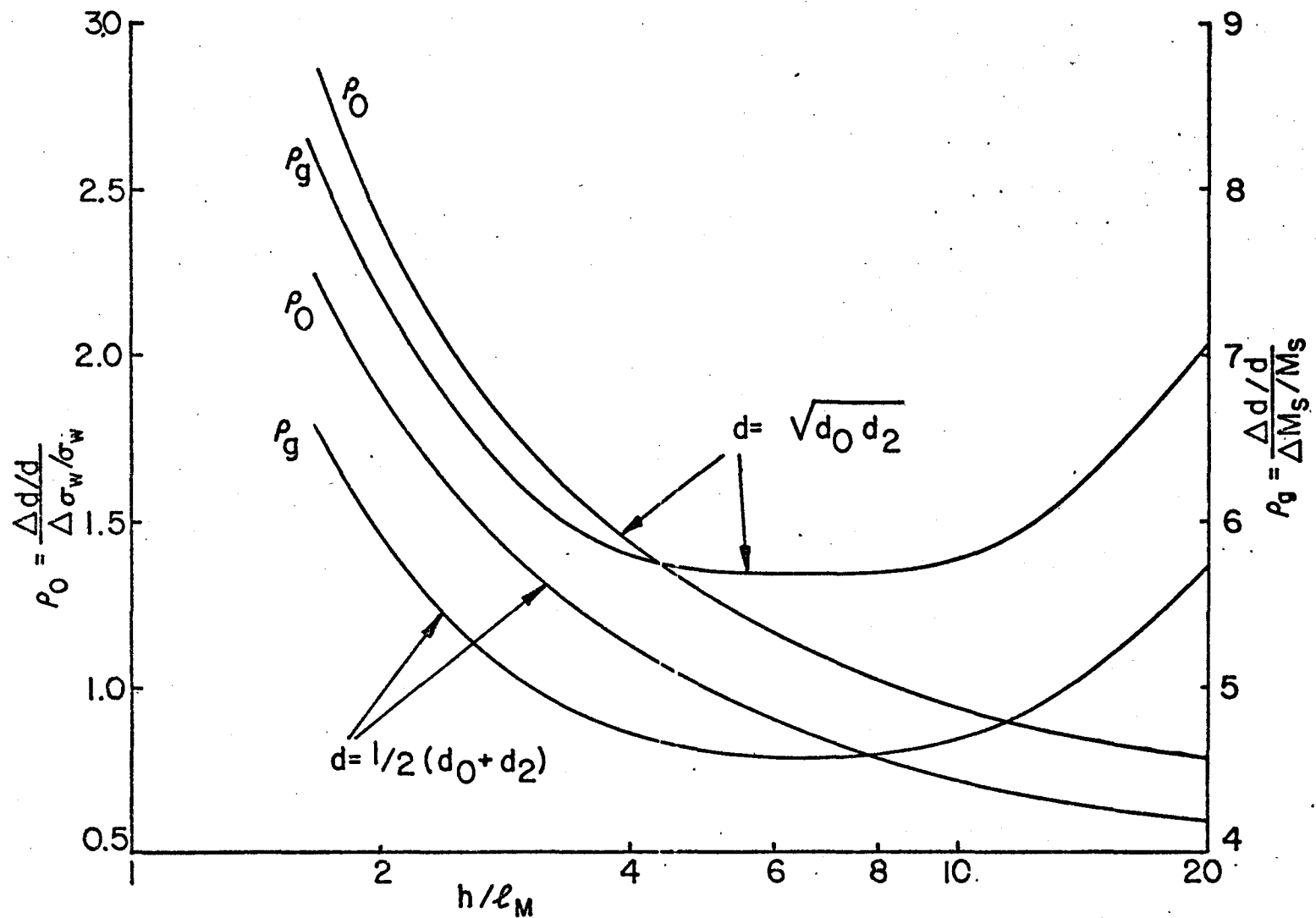


Fig. 4.1: The temperature sensitivities of bubble diameters for the mixed rare-earth orthoferrites and the uniaxial garnets as a function of plate thickness for 2 bias conditions.

Furthermore, for garnets there exists an optimum plate thickness of approximately  $6\ell_M$  for minimum  $\rho_g$ . This minimum is fairly flat permitting operation at the optimum described by Thiele of  $4\ell_M$ . For the mixed rare-earth orthoferrites, the curves decrease monotonically with thickness, indicating it is desirable to have as thick a plate as possible subject to other constraints. As an illustrative example, if one uses a plate whose thickness is say  $6.5\ell_M$ , then the bubble diameter will be 4% larger than Thiele's optimum bubble given by equation (2.10), while  $\rho_0$  will be 30% smaller.

It is also suggested that the optimum bias condition for a bubble is the arithmetic mean since not only does one obtain greater field margins than with the geometric mean, but also less temperature sensitivity.

#### 4.4 Zero Temperature Sensitivity of Bubble Domains

In some of the uniaxial garnets recently developed, both the magnetization and the wall-energy density vary with temperature<sup>41</sup>. Thus, it can be seen from equations (4.17) and (4.20) that for materials whose wall-energy densities as well as magnetizations vary positively with temperature, the total change in bubble diameter will be

$$\frac{\Delta d}{d} = \rho_0 \frac{\Delta \sigma_w}{\sigma_w} - \rho_g \frac{\Delta M_s}{M_s} \quad (4.23a)$$

$$= \left( \frac{\ell_M/h}{S_0(a) - \ell_M/h} \right) \frac{\Delta \sigma_w}{\sigma_w} \left( \frac{F(a) + \ell_M/h}{S_0(a) - \ell_M/h} \right) \frac{\Delta M_s}{M_s} \quad (4.23b)$$

Smith and Anderson<sup>41</sup> suggested that in order to obtain a fixed bubble size with temperature,  $\ell_M$  should be temperature independent. In this case, for incremental increases of  $\Delta\sigma_w$  and  $\Delta M_s$  in the wall-energy and magnetization respectively, the material characteristic length defined by equation (2.1) will be given by

$$\ell_M + \Delta\ell_M = \frac{\sigma_w + \Delta\sigma_w}{4\pi(M_s + \Delta M_s)^2} \quad (4.24)$$

Neglecting second and higher order terms, equation (4.24) becomes

$$\ell_M + \Delta\ell_M \approx \frac{\sigma_w}{4\pi M_s^2} \left(1 + \frac{\Delta\sigma_w}{\sigma_w} - \frac{2\Delta M_s}{M_s}\right) \quad (4.25)$$

Subtracting equation (2.1) from equation (4.25) yields,

$$\frac{\Delta\ell_M}{\ell_M} \approx \frac{\Delta\sigma_w}{\sigma_w} - \frac{2\Delta M_s}{M_s} \quad (4.26)$$

Thus, the condition for zero temperature change in  $\ell_M$  is

$$\frac{\Delta\sigma_w}{\sigma_w} = \frac{2\Delta M_s}{M_s} \quad (4.27)$$

However, it can be seen from equation (4.23b) that the condition for zero temperature sensitivity of bubble diameter is given by

$$\frac{\Delta\sigma_w/\sigma_w}{\Delta M_s/M_s} = 1 + \frac{hF(a)}{\ell_M} \quad (4.28)$$

Noting that  $F(a)$  is given by equation (2.9),

$$F(a) = \ell_M/h + aH/4\pi M_s \quad (2.9)$$

Therefore,

$$\frac{\Delta\sigma_w/\sigma_w}{\Delta M_s/M_s} = 2 + \left(\frac{ah}{\ell_M}\right) \frac{H}{4\pi M_s} \quad (4.29)$$

Consequently,

$$\Delta\sigma_w/\sigma_w > 2 \frac{\Delta M_s}{M_s} \quad (4.30)$$

Equation (4.28) was used to calculate  $\frac{\Delta\sigma_w/\sigma_w}{\Delta M_s/M_s}$  as a function of plate thickness and bubble diameter. Fig. 4.2 shows a plot of  $\frac{\Delta\sigma_w/\sigma_w}{\Delta M_s/M_s}$  as a function of plate thickness for the two bias conditions

$$d = \sqrt{d_0 d_2} \quad \text{and} \quad d = \frac{1}{2}(d_0 + d_2) .$$

In Fig. 4.3,  $\frac{\Delta\sigma_w/\sigma_w}{\Delta M_s/M_s}$  is plotted as a function of bubble diameter for several plate thicknesses. Thus, Figs. 4.2 and 4.3 can be used to select the appropriate uniaxial material which will give zero temperature sensitivity of bubble domains in a bubble device if the operating conditions are known. In order to make both  $d$  and  $\ell_M$  temperature independent, it is preferable to operate as close as possible to the conditions given by equation (4.27). As can be seen from Figs. 4.2 and 4.3, it is therefore preferable to use as thin a plate as possible subject to other constraints.

#### 4.5 Conclusion

A method for measuring the temperature dependence of  $\sigma_w$  in orthoferrites and  $M_s$  in some garnets that use a single bubble domain without the need to collapse the bubble in order to obtain the measurement has been described. The temperature sensitivities of bubble

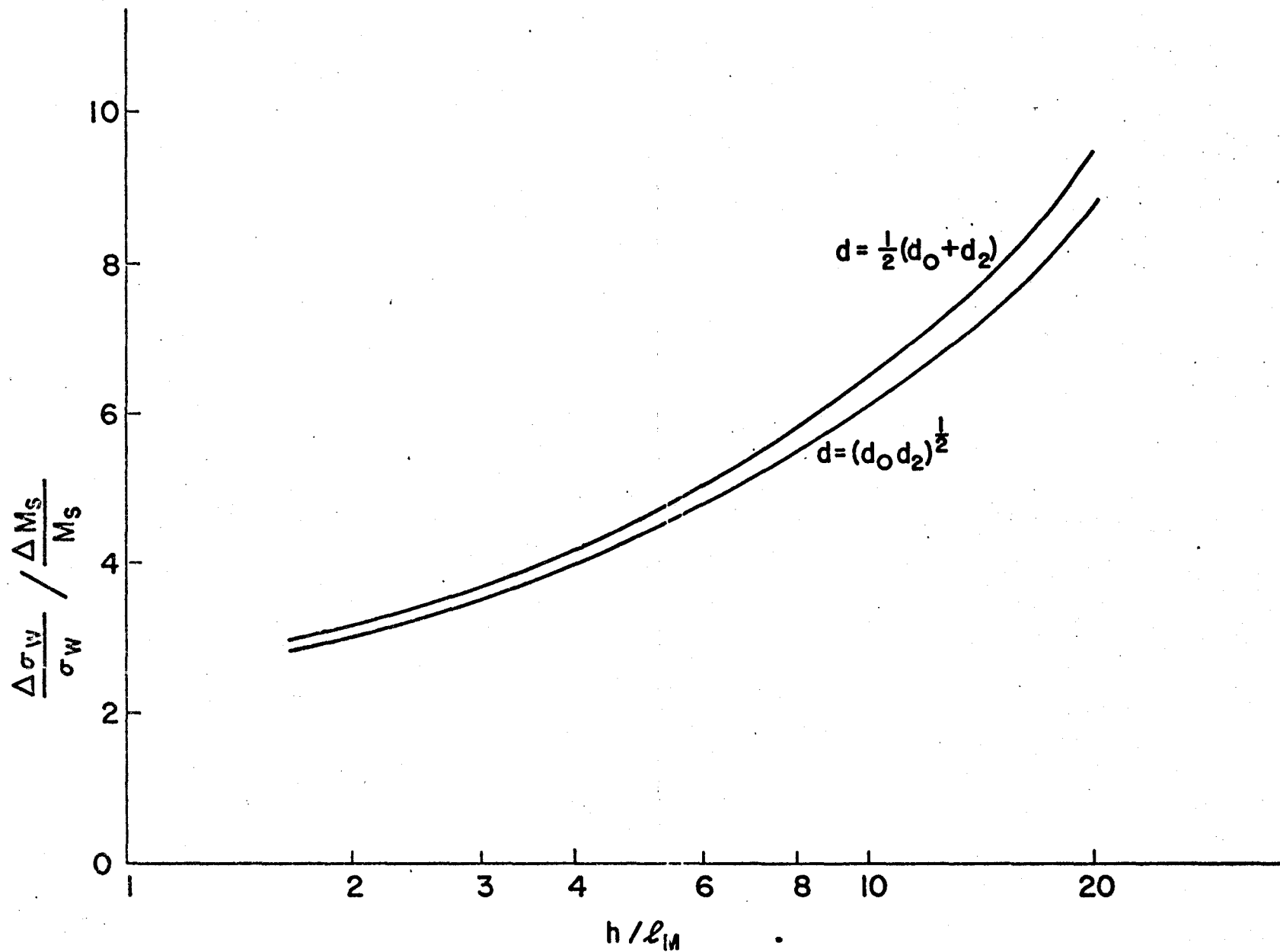


Fig. 4.2: The ratio of the fractional changes in wall energy density and magnetization for zero temperature sensitivity as a function of plate thickness for two bias conditions.

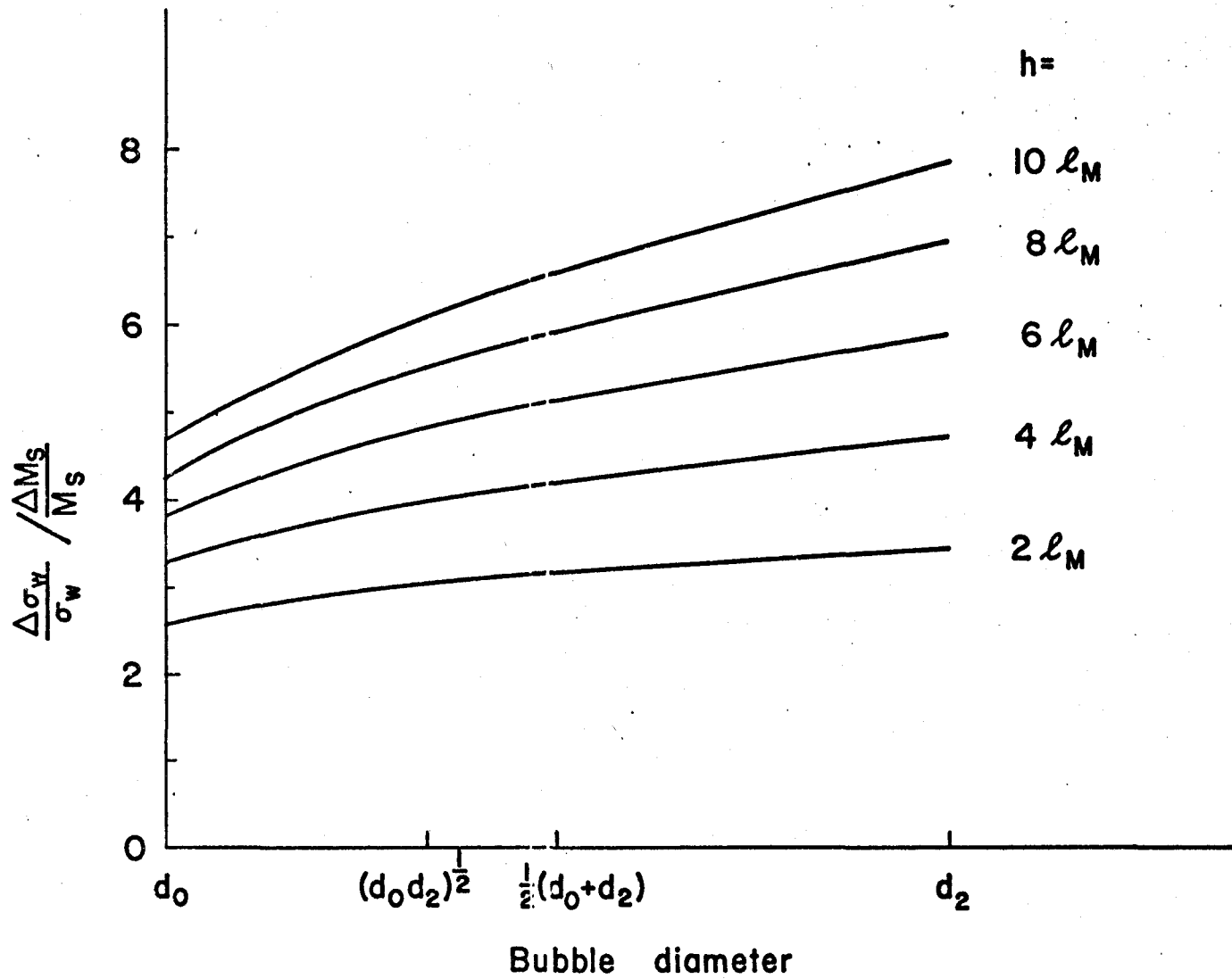


Fig. 4.3:  $\frac{\Delta\sigma_w/\sigma_w}{\Delta M_s/M_s}$  as a function of bubble diameter for several plate thicknesses.

domains in the mixed rare-earth orthoferrites and the uniaxial garnets have been derived in terms of the material parameters. For the garnets, there exists an optimum plate thickness of  $6l_M$  to minimize the sensitivity, although this minimum is fairly flat from  $4l_M$  to  $10l_M$ . For the orthoferrites, it is preferable to use as thick a plate as possible subject to other constraints. The condition for zero temperature sensitivity of bubble domains in some uniaxial materials has also been obtained, and can be used in designing bubble devices having fixed bubble size with temperature fluctuations.

## CHAPTER V

### CUTTING STRIP AND BUBBLE DOMAINS

#### 5.0 Introduction

Bubble domains can be generated in bubble devices by cutting a bubble from a strip domain or from another bubble. Two methods can be used to do this. The first method utilizes the poles induced in a thin permalloy overlay circuit known as a bubble generator<sup>33</sup> by means of an in plane rotating magnetic field, while the second method uses a current flowing through a conductor touching the surface of the platelet<sup>4,5</sup>. In a practical bubble device, it is important to be able to predict the cutting field when the material parameters are known. Thus, a study of the current requirement to cut a bubble from a strip domain in uniaxial platelets was carried out both experimentally and theoretically and is reported in this chapter. A theoretical study was also made of the field required to cut a bubble domain from another bubble. This work has been reported by the author in Refs. 23, 24 and 26.

#### 5.1 Cutting Strip Domains by Use of Electric Currents

The strip domains were cut by means of a pulsed current flowing through a 25 $\mu$ m gold wire touching the platelet surface and placed at right angles to the strip domain walls. The electric current was supplied by a Chronetics PG-13A pulse generator and measured using a Tektronix P6021 current probe. The widths of the strip domains were varied by

changing the bias field and measured accurately, using the Faraday effect, by means of a calibrated reticule.

The average magnetic field on the domain wall due to a current  $I$  flowing through a wire of radius  $r$  touching the platelet and at right angles to the wall is

$$\bar{H}_z = \frac{1}{h} \int_0^h H_z dz \quad (5.1)$$

where  $H_z$  is the vertical component of the magnetic field at a point on the domain wall at a horizontal distance  $a$  from the center of the wire. Therefore, equation (5.1) becomes

$$\bar{H}_z = \frac{1}{h} \int_0^h \frac{Ia}{2\pi[a^2+(r+z)^2]} dz \quad (5.2)$$

$$= \frac{I}{2\pi h} \left[ \tan^{-1}\left(\frac{h+r}{a}\right) - \tan^{-1}\left(\frac{r}{a}\right) \right] \quad (5.3)$$

The cutting field  $H_r$  will then be given by

$$H_r = \frac{I_r}{2\pi h} \left[ \tan^{-1}\left(\frac{h+r}{a}\right) - \tan^{-1}\left(\frac{r}{a}\right) \right] + H \quad (5.4)$$

where  $I_r$  is the cutting current, and  $H$  is the bias field.

Measurements of the cutting field obtained from equation (5.4) as a function of strip width  $2b$  were carried out on an  $8\ell_M$  thick plate of  $\text{Sm}_{0.55}\text{Tb}_{0.45}\text{FeO}_3$  ( $4\pi M_s = 108$  EMU), and a  $6\ell_M$  thick plate of  $\text{TbFeO}_3$  ( $4\pi M_s = 138$  EMU). The results of these measurements are represented by circles and crosses respectively on Fig. 5.1.

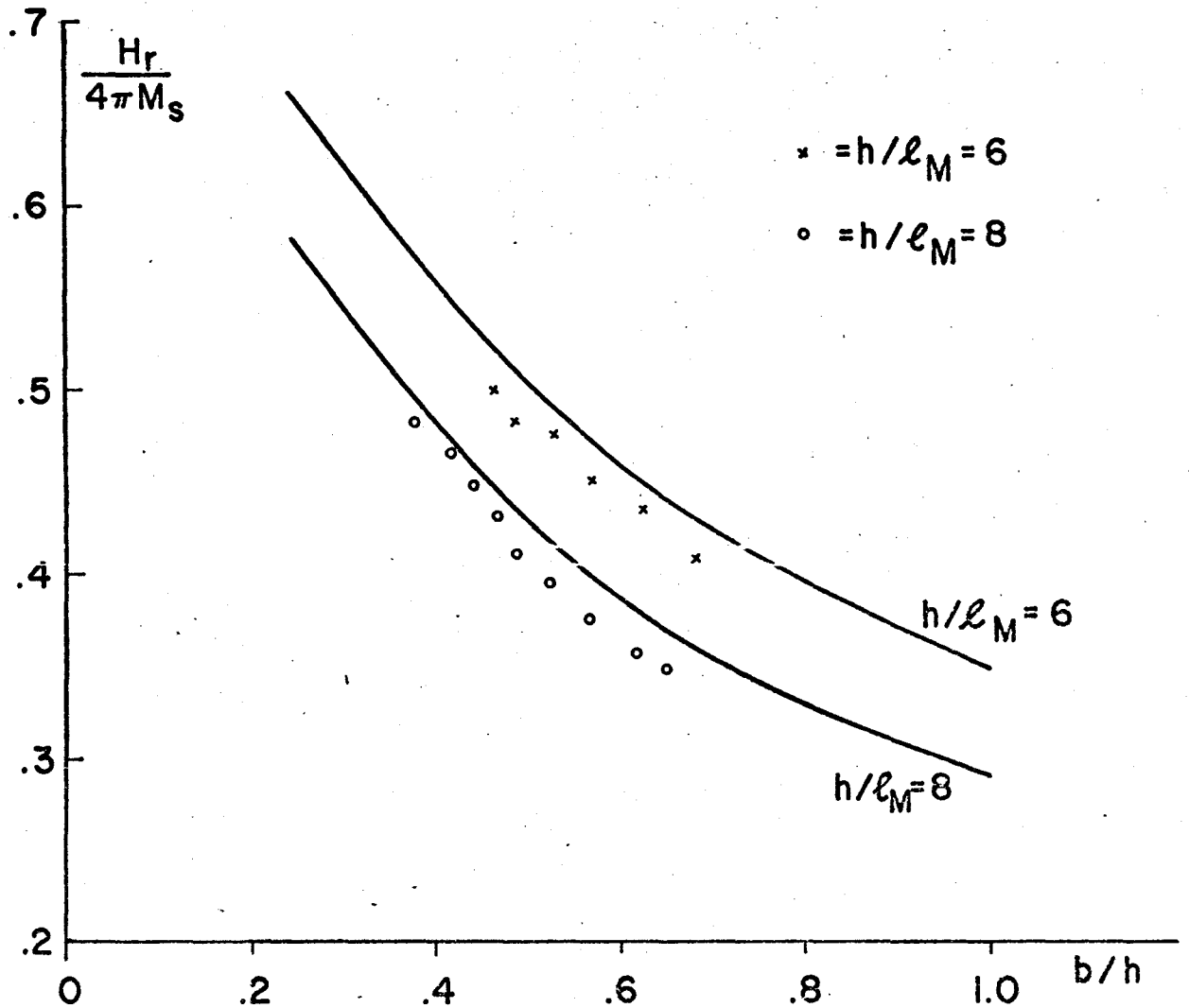


Fig. 5.1: Experimental and theoretical cutting field as a function of half strip width for a  $6\ell_M$  thick plate of  $\text{TbFeO}_3$  and an  $8\ell_M$  thick plate of  $\text{Sm}_{0.55}\text{Tb}_{0.45}\text{FeO}_3$ .

According to Della Torre<sup>18</sup>, the average value of the magnetic field at a point on the domain wall due to the magnetization  $\bar{H}_M$  is given by

$$\frac{\bar{H}_M}{4\pi M_s} = \frac{1}{4} + \frac{1}{\pi} \int_0^1 \frac{du}{u^2} \ln \left[ \frac{g + \sqrt{(1-u)^2 + g^2}}{g + \sqrt{(1-u)^2 + g^2 + u^2}} \right] \quad (5.5)$$

where

$$g(u) = \frac{u}{h} f\left(\frac{h(1-u)}{u}\right) \quad (5.6)$$

The function  $f(x)$ , where  $x = \frac{h(1-u)}{u}$  represents the equation of the domain wall in cartesian coordinates.

It may be noted that the integrand in equation (5.5) has a singularity at  $u=1$  and is indeterminate, but approaches zero at  $u=0$ . Thus care must be taken in carrying out the integration numerically. The Runge-Kutta method was used in all the numerical computations.

The minimum field required to produce the cutting will be equal to the sum of  $\bar{H}_M$  given by equation (5.5) and an equivalent field to overcome the pressure due to wall energy  $H_{eq}$  given by

$$\frac{H_{eq}}{4\pi M_s} = \frac{\ell_M}{2R} \quad (5.7)$$

where  $R$  is the radius of curvature of the point of cutting, and can be obtained from the formula

$$R = \frac{[1 + (dy/dx)^2]^{3/2}}{d^2y/dx^2} \quad (5.8)$$

Several functions were used to simulate the shape of the upper domain wall just before cutting occurs. It was found that the "Cauchy" type

function used by Della Torre<sup>18</sup> [ $f(x) = bx^2/[(x-a)^2 + a^2]$ ] has a large radius of curvature at the point of cutting, but the notch area (defined in Fig. 5.2) is also large, giving much larger values for the cutting field than observed experimentally. The "Gauss" type function [ $f(x) = b + \frac{b}{a}(x-a)\exp[-(x-a)^2/2a^2 - \frac{1}{2}]$ ] on the other hand has a small notch area, but the radius of curvature at the point of cutting is small, giving values for the cutting field close to those obtained by the "Cauchy" function. Various other functions, including sinusoidal and higher order "Cauchy" and "Gauss" type functions were tried and all exhibited similar problems. The normalized cutting fields for  $h=8\ell_M$  and  $b=h$  calculated from the various functions that were used to simulate the domain wall shape at the instant of cutting are given in Table 5.1 for comparison. A domain wall shape that has both a large radius of curvature and at the same time a small notch area consists of sections of ellipses and straight lines given by

$$\begin{aligned}
 f(x) &= b & x &\leq -a \\
 f(x) &= b[1 - \sqrt{1-x^2/a^2}] & -a &\leq x \leq a \\
 f(x) &= b[1 + c/b\sqrt{1-(x-2a)^2/a^2}] & -a &\leq x \leq 3a \\
 f(x) &= b & x &\geq 3a
 \end{aligned} \tag{5.9}$$

The corners of the curves have been rounded off to obtain a continuous curve. The resulting curve and its image corresponding to the lower domain wall are shown in Fig. 5.2. It may be noted that the sections of ellipses need not be symmetrical about the line  $x=a$ , where the current

Table 5.1: Normalized Cutting Field for  $b=h$  and  $h=8\ell_M$  Calculated from Several Functions

| Function                 | Equation of Domain Wall<br>$f(x)$   | Radius of<br>Curvature R | Notch Area<br>(See Fig. 5.2)                   | Normalized Cutting<br>field $H_r/4\pi M_s$<br>at $h=8\ell_M, b=h$ |
|--------------------------|---|--------------------------|--|---|
| Cauchy                   | $bx^2/[(x-a)^2+a^2]$  | $a^2/b$                  | $\infty$                                       | 0.635   |
| Gaussian                 | $b+b/a(x-a)\exp-[(x-a)^2/2a^2-1/2]$   | $a^2/2b$                 | $abe^{1/2}$                                    | 0.615   |
| Higher order<br>Cauchy   | $b[1 + \frac{16}{9} \frac{a(x-a)^3}{[(x-a)^2+a^2/3]^2}]$  | $2a^2/3b$                | $\infty$                                       | 0.475   |
| Higher order<br>Gaussian | $b+b/a(x-a)\exp-[(x-a)^4/4a^4-1/4]$   | $a^2/4b$                 |  | 0.45  |
| Sinusoidal               | $\left. \begin{array}{l} b \quad x \leq -a \\ b[1+\sin \frac{\pi(x-a)}{2a}] \quad -a \leq x \leq a \\ b \quad x \geq a \end{array} \right\}$  | $4a^2/\pi^2b$            | $2ab/\pi$                                      | 0.595   |
| Symmetrical<br>ellipses  | $\left. \begin{array}{l} b \quad x \leq -a \\ b[1 - \sqrt{1-x^2/a^2}] \quad -a \leq x \leq a \\ b[1 + \sqrt{1-(x-2a)^2/a^2}] \quad a \leq x \leq 3a \\ b \quad x \geq 3a \end{array} \right\}$    | $a^2/b$                  | $\frac{\pi}{2} ab$                             | 0.27  |
| Asymmetrical<br>ellipses | $\left. \begin{array}{l} b \quad x \leq -a \\ b[1 - \sqrt{1-x^2/a^2}] \quad -a \leq x \leq a \\ b[1 + c/b\sqrt{1-(x-2a)^2/a^2}] \quad a \leq x \leq 3a \\ b \quad x \geq 3a \end{array} \right\}$ | $a^2/b$<br>or<br>$a^2/c$ | $\frac{\pi}{2} ab$<br>or<br>$\frac{\pi}{2} ac$ | 0.29  |

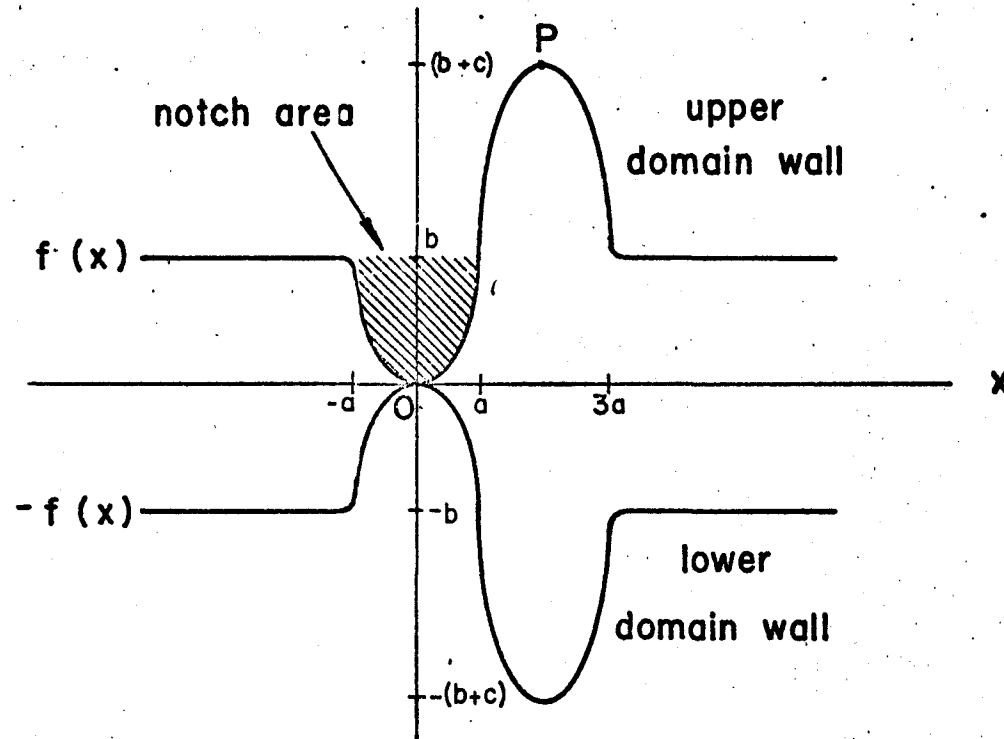


Fig. 5.2: Shape of strip domain at instant of cutting.

carrying wire is located. The field due to the current drives the walls apart for  $x > a$  and pushes them together for  $x < a$ . Thus, cutting takes place at the origin when the total field on the wall at the origin is equal to or exceeds the cutting field.

To ensure that the point P in Fig. 5.2 is in equilibrium at the instant of cutting the ratio  $c/b$  was determined at each value of plate thickness and strip width which makes the cutting field calculated at point O equal to the field calculated at P. As an illustrative example, when  $b=h$  and  $h=8\ell_M$ , it was found that a value of  $c = 0.3b$  makes both fields equal. Thus,  $\bar{H}_M$ ,  $H_{eq}$  and  $\bar{H}_M + H_{eq}$  calculated at points O and P are plotted as a function of  $a/h$  in Figs. 5.3(a) and 5.3(b), respectively. It is seen that cutting occurs when  $a/h = 0.6$ , and the cutting field  $H_r$  is equal to  $0.29 \times 4\pi M_s$ .

The cutting field was computed as a function of  $b/h$  for plates of thickness  $6\ell_M$  and  $8\ell_M$  and represented in Fig. 5.1 by the solid lines. It can be seen that the agreement with the experimental values is good. Fig. 5.4 shows  $c/b$  as a function of  $b/h$  for  $h=6\ell_M$  and  $h=8\ell_M$ . It is interesting to note that for both thicknesses  $c/b$  was found to vary linearly with  $b/h$ .

## 5.2 Replication of Bubble Domains

A theoretical study of magnetic field required to replicate bubble domains has been made. The domain wall at the instant of cutting was considered to consist of sections of ellipses and circles given by:

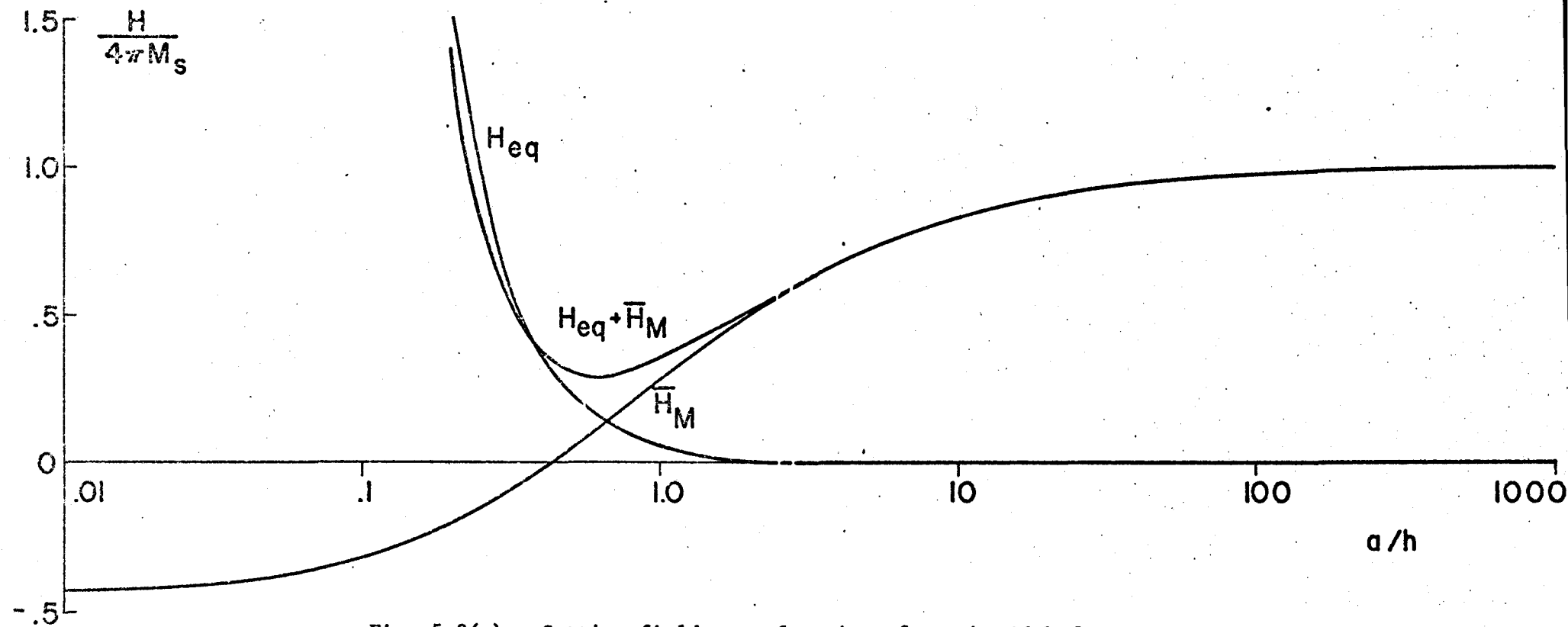


Fig. 5.3(a): Cutting field as a function of notch width for  $h=8\ell_M$  and  $b=h$  at point 0 in Fig. 5.2.

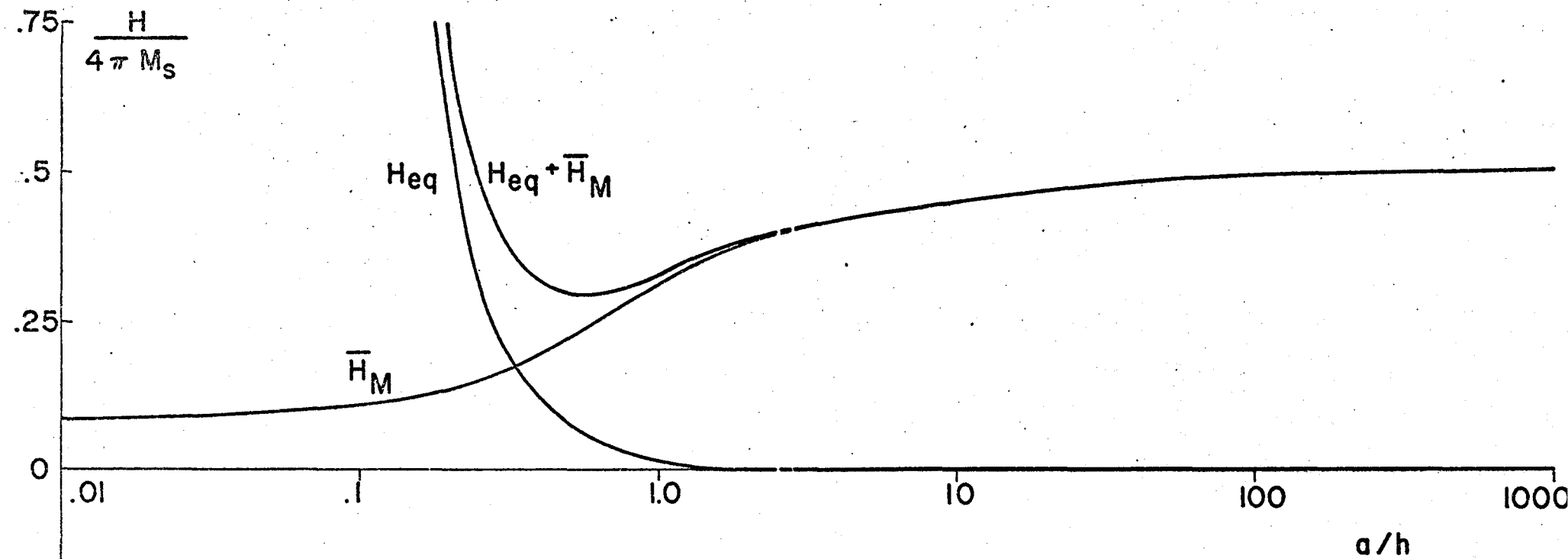


Fig. 5.3(b): Cutting field as a function of notch width for  $h=8\ell_M$  and  $b=h$  at point P in Fig. 5.2.

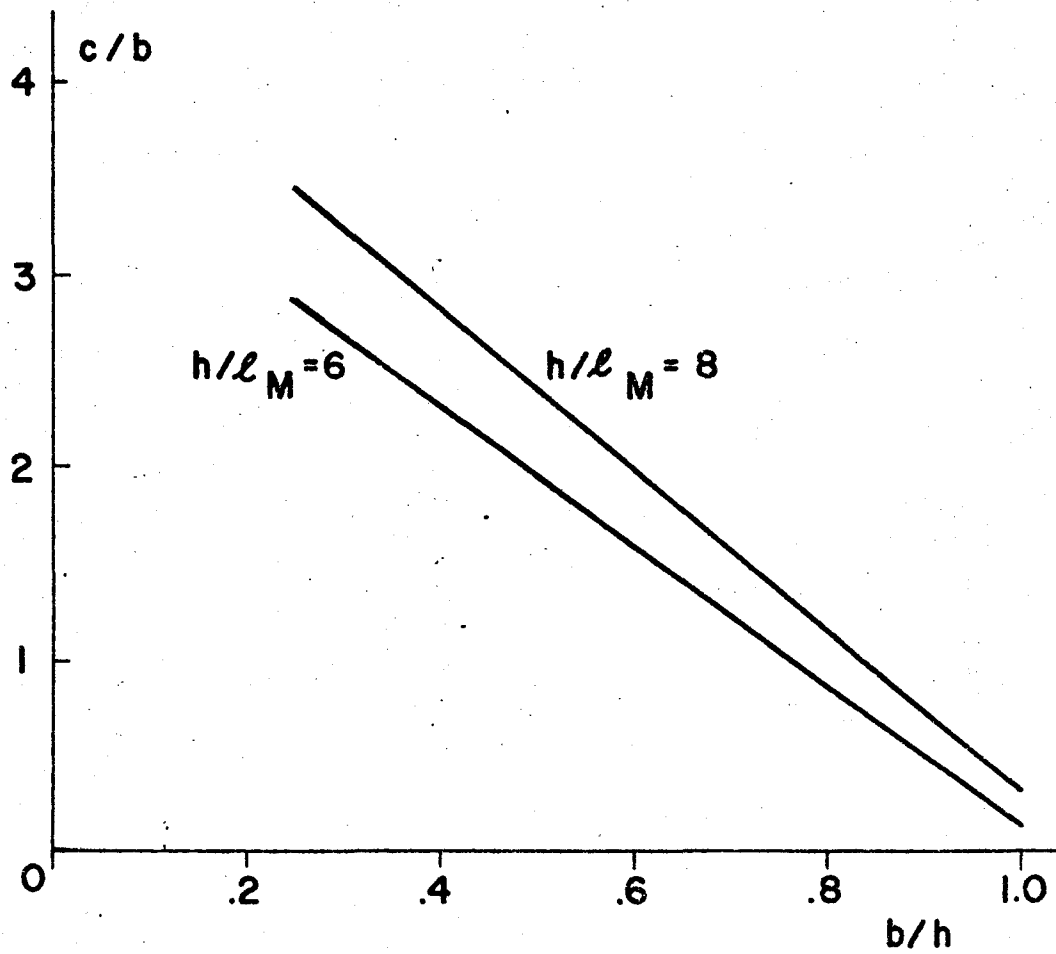


Fig. 5.4:  $c/b$  as a function of  $b/h$  for  $h=6l_M$  and  $8l_M$ .

$$\begin{aligned}
 f(x) &= \sqrt{b^2 - (x+a)^2} & -(a+b) \leq x \leq -a \\
 f(x) &= b[1 - \sqrt{1 - x^2/a^2}] & -a \leq x \leq a \\
 f(x) &= b[1 + c/b \sqrt{1 - (x-2a)^2/a^2}] & a \leq x \leq 3a \\
 f(x) &= \sqrt{b^2 - (x-3a)^2} & 3a \leq x \leq (3a+b)
 \end{aligned}
 \tag{5.10}$$

The resulting curve and its image corresponding to the lower domain wall are shown in Fig. 5.5. This domain wall shape is somewhat similar to the one considered in Section 5.1 (represented by equation (5.9)) to study the current required to cut a strip domain. The difference is that both ends of the shape represented by equation (5.9) have been terminated by circles in order to depict the shape of the bubble walls just before cutting takes place.

The method for obtaining the cutting field described in Section (5.1) was employed to calculate the bubble replication field as a function of plate thickness and bubble diameter. The results of these calculations are plotted in Figs. 5.6 and 6.7.

It can be seen from Figs. 5.1, 5.6 and 5.7 that a larger cutting field is required to cut a bubble from another bubble. As an illustrative example, for  $h=8\ell_M$  and  $b=h$ , a field approximately equal to  $0.6 \times (4\pi M_s)$  is required to replicate a bubble domain, while the field required to cut a strip domain is only  $0.29 \times (4\pi M_s)$ .

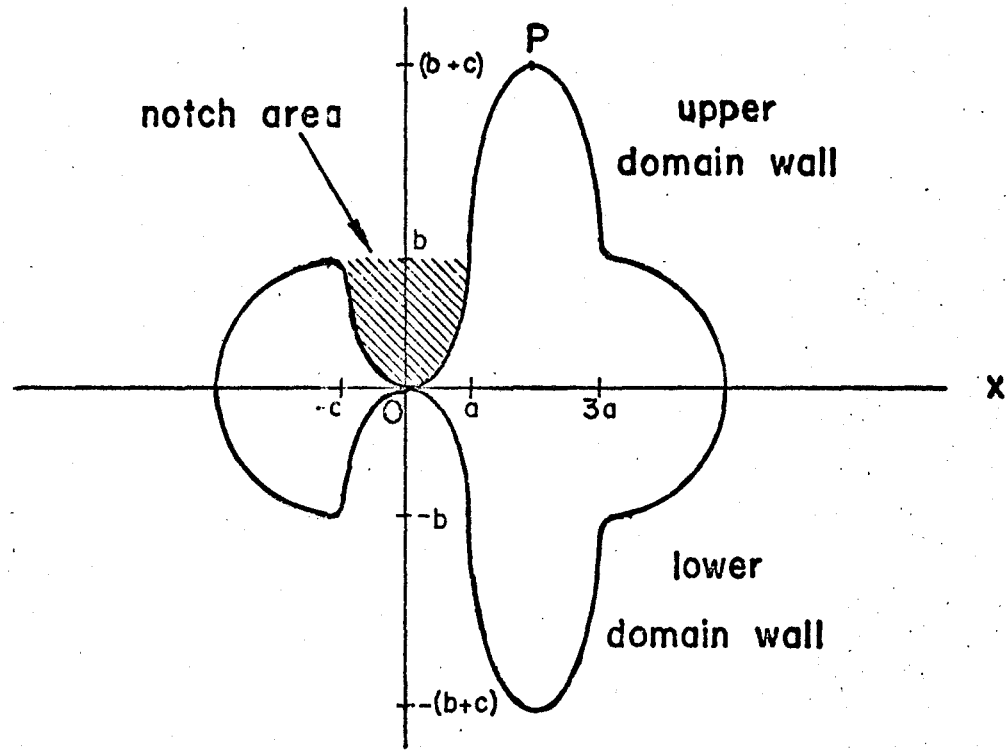


Fig. 5.5: Shape of bubble domain at instant of cutting.

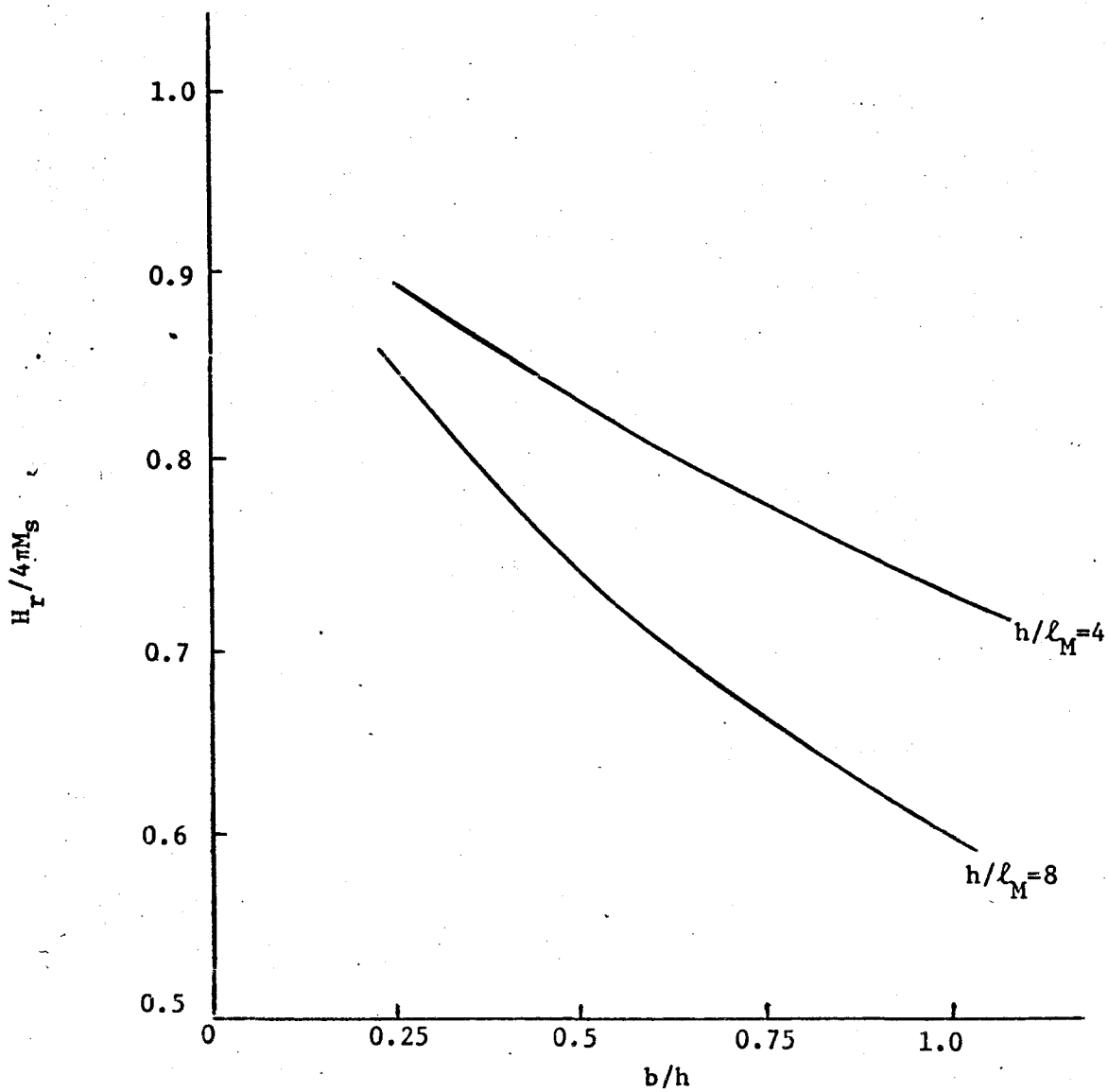


Fig. 5.6: Bubble replication field as a function of  $b/h$  for two plate thicknesses.

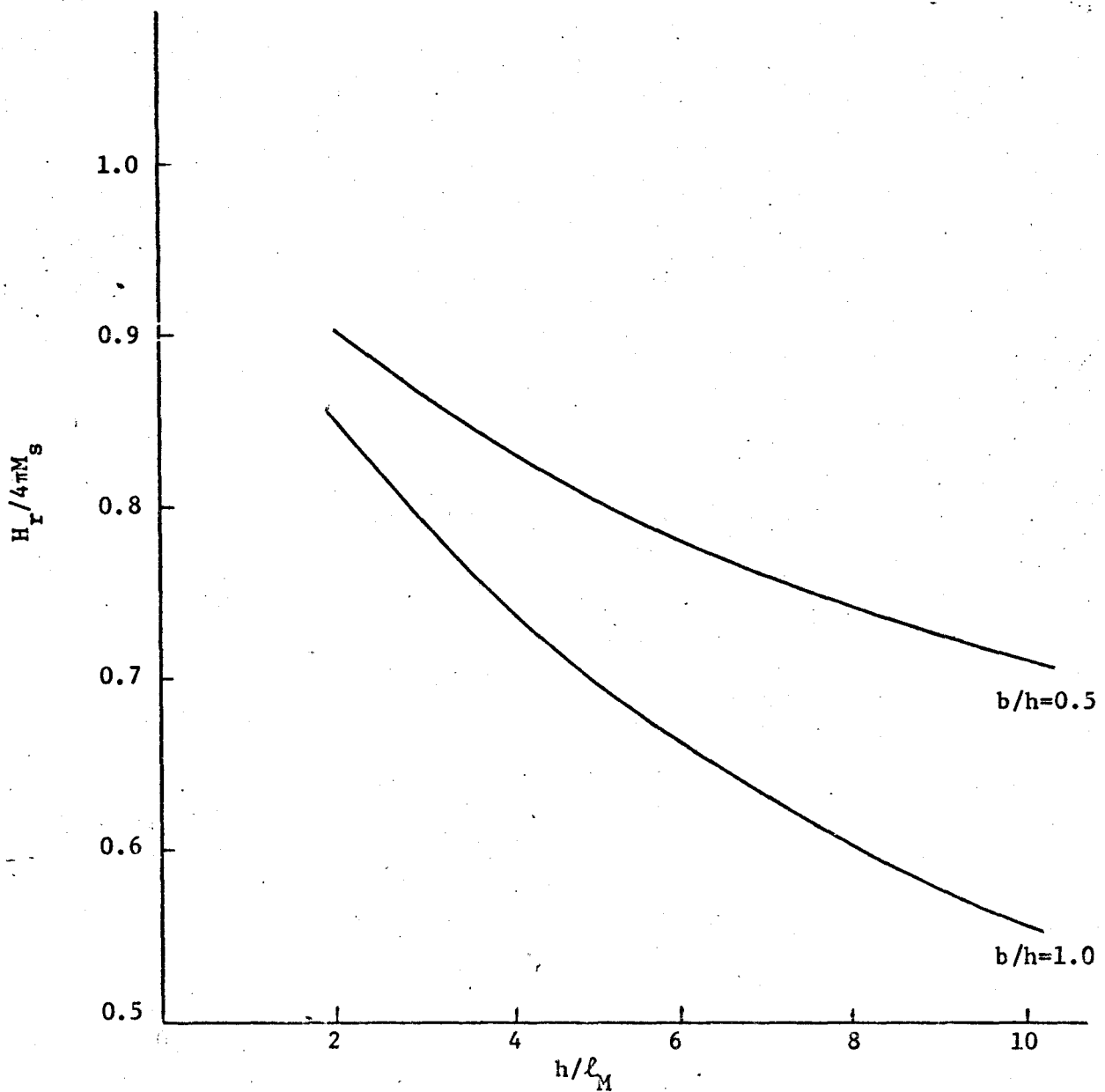


Fig. 5.7: Bubble replication field as a function of plate thickness.

### 5.3 Conclusions

An experimental and theoretical investigation of the current required to cut a strip domain has been reported in this chapter. It was shown that a good agreement between the theoretical and experimental results is obtained when the wall is considered to consist of sections of ellipses and straight lines just before cutting occurs. Also, a theoretical study of the field required to replicate a bubble domain has been presented.

The work reported in this chapter completes the first phase of a study of current requirements to cut strip and bubble domains. More work is required to study the various other structures that can be used to generate bubbles in bubble devices. An example is the optimization of the hairpin-type conductor bubble generator, which is normally used in current-access bubble devices.

## CHAPTER VI

### CONCLUSIONS

Possible device applications for bubble domains in uniaxial magnetic materials have spurred interest in investigating these materials both theoretically and experimentally in order to obtain a better understanding of these materials and their complex domain structure. Thus, a study of domain walls in some uniaxial materials has been undertaken and presented in this thesis.

It has been shown that the anisotropy of wall energy in orthoferrites causes bubble domains to be elliptical. A formula relating the eccentricity of an elliptical bubble to the anisotropic wall energy has been derived, and an experimental technique for measuring the wall anisotropy has been described. In  $\text{Sm}_{0.55}\text{Tb}_{0.45}\text{FeO}_3$  a measured anisotropy energy of 1.7% of the average wall-energy density at room temperature is responsible for eccentricities as large as 0.4 of average bubble radii equal to 85% of the bubble strip-domain transition radius. In attempting to explain wall anisotropy physically, it was suggested that in orthoferrites walls parallel to the a axis are Bloch walls, while walls parallel to the b axis are Néel walls. To investigate this hypothesis, the wall-energy anisotropy was measured as a function of the quality factor  $q$  by varying the temperature of the sample. The measurements seem to verify the predicted dependence of wall anisotropy on  $q$  and the hypothesis.

Methods for obtaining the temperature dependence of the material characteristic length for the mixed rare-earth orthoferrites and the garnets using an isolated bubble domain without collapsing it have been developed. These methods led to the derivation of the temperature sensitivities of bubble domains in the rare-earth orthoferrites and the garnets in terms of the material parameters. It was found that for garnets there exists an optimum plate thickness of  $6l_M$  to minimize the sensitivity, although this minimum is fairly flat from  $4l_M$  to  $10l_M$ . For the orthoferrites on the other hand, it is preferable to use as thick a plate as possible subject to other constraints. For both materials, it was found that a smaller temperature sensitivity is obtained when the arithmetic mean diameter is used as the bias condition. The condition for zero temperature sensitivity of bubble domains in some uniaxial garnets has been obtained in terms of the material parameters. The ratio of the fractional changes in wall energy density and saturation magnetization which gives zero temperature sensitivity has been plotted as a function of plate thickness and bubble diameter. The resulting curves can be used in designing bubble devices having fixed bubble sizes.

Finally, a study of the current requirement to cut a bubble from a strip domain in uniaxial plates has been carried out both experimentally and theoretically. Various functions have been used to simulate the shape of the walls at the instant of cutting. It was found that good agreement with the measured values of cutting field is obtained when the wall shape was considered to consist of sections of

ellipses and straight lines. Also, a theoretical study of the field required to replicate a bubble domain has been made and the results given.

#### REFERENCES

1. Almasi, G.S., Keefe, G.E., Lin, Y.S., and Thompson, D.A., "A magnetoresistive detector for bubble domains" J. Appl. Phys., vol. 42, March 1971, pp. 1268-1269.
2. Almasi, G.S., "Magneto optic bubble-domain devices", IEEE Trans. Magn., vol. MAG-7, Sept. 1971, pp. 370-373.
3. Almasi, G.S., Bouricius, W.G., and Carter, W.C., "Reliability and organization of a  $10^8$ -bit bubble domain memory", AIP Conf. Proc., No. 5, 1972, pp. 225-229.
4. Bobeck, A.H., "Properties and device applications of magnetic domains in orthoferrites", Bell Syst. Tech. J., vol. 46, Oct. 1967, pp. 1901-1925.
5. Bobeck, A.H., Fischer, R.F., Perneski, A.J., Remeika, J.P., and Van Uitert, L.G., "Application of orthoferrites to domain wall devices", IEEE Trans. Magn., vol. MAG-5, Sept. 1969, pp. 544-553.
6. Bobeck, A.H., Spencer, E.G., Van Uitert, L.G., Abrahams, S.C., Barns, R.L., Grodkiewicz, W.H., Sherwood, R.C., Schmidt, P.H., Smith, D.H., and Walters, E.M., "Uniaxial magnetic garnets for domain wall bubble devices", Appl. Phys. Lett., vol. 17, 1970, p. 131.

7. Bobeck, A.H., and Scovil, H.E.D., "Magnetic Bubbles", Sci. Am., vol. 224, June 1971, pp. 78-90.
8. Bobeck, A.H., Smith, D.H., Spencer, E.G., Van Uitert, L.G., and Walters, E.M., "Magnetic properties of flux grown uniaxial garnets", IEEE Trans. Magn., vol. MAG-7, Sept. 1971, pp. 461-463.
9. Bobeck, A.H., Fischer, R.F., and Smith, J.L., "An overview of magnetic bubble domains - material-device interface", AIP Conf. Proc., No. 5, 1971, pp. 45-55.
10. Bonyhard, P.I., Danylchuk, I., Kish, D.E., and Smith, J.L., "Applications of bubble devices", IEEE Trans. Magn., vol. MAG-6, Sept. 1970, pp. 447-451.
11. Burrington, R.S., Handbook of Mathematical Tables and Formulas, 3rd ed., New York: McGraw-Hill, 1962, p. 29.
12. Chikazumi, S., Physics of Magnetism, New York, John Wiley & Sons, Inc., 1966.
13. Clover, Jr., R.B., Wentworth, C., and Mroczkowski, S.S., "Low birefringent orthoferrites for optical devices", IEEE Trans. Magn., vol. MAG-7, Sept. 1971, pp. 480-483.
14. Copeland, J.A., Elward, J.P., Johnson, W.A., and Ruch, J.G., "Single-conductor magnetic-bubble propagation circuits", J. Appl. Phys., vol. 42, March 1971, pp. 1266-1267.

15. Danylchuk, I., "Operational characteristics of 1024 bit garnet bubble Y-bar shift register", J. Appl. Phys., vol. 42, March 1971, pp. 1358-1359.
16. Della Torre, E., and Dimyan, M.Y., "Anisotropy of wall energy in orthoferrites", Int. Magnetism Conf., Washington, D.C., April 1970.
17. Della Torre, E., and Dimyan, M.Y., "Anisotropy of wall energy in orthoferrites", IEEE Trans. Magn., vol. MAG-6, Sept. 1970, pp. 489-492.
18. Della Torre, E., "Pressures on cylindrical magnetic domain walls", IEEE Trans. Magn., vol. MAG-6, Dec. 1970, pp. 822-827.
19. Dimyan, M.Y., and Della Torre, E., "Temperature dependence of wall-energy anisotropy in orthoferrites", Int. Magnetism Conf., Denver, Colo., April 1971.
20. Dimyan, M.Y., and Della Torre, E., "Temperature dependence of wall-energy anisotropy in orthoferrites", IEEE Trans. Magn., vol. MAG-7, Sept. 1971, pp. 476-479.
21. Dimyan, M.Y., and Della Torre, E., "A method for measuring the temperature dependence of the magnetization in uniaxial garnets", Proc. IEEE, vol. 59, Nov. 1971, pp. 1623-1624.
22. Dimyan, M.Y., and Della Torre, E., "Temperature sensitivity of bubble domains", J. Appl. Phys., vol. 43, Mar. 1972, pp. 1285-1287.

23. Dimyan, M.Y., and Della Torre, E., "Cutting strip domains by use of electric currents", Int. Magnetism Conf., Kyoto, Japan, April 1972.
24. Dimyan, M.Y., and Della Torre, E., "Cutting strip domains by use of electric currents", Submitted to IEEE Trans. Magn.
25. Dimyan, M.Y., and Della Torre, E., "Zero temperature sensitivity of bubble domains", Submitted to J. Appl. Phys.
26. Dimyan, M.Y., and Della Torre, E., "A study of bubble replication", Submitted to IEEE Trans. Magn.
27. Fowles, D.C., and Copeland, J.A., "Rapid method for determining the magnetization and intrinsic length of magnetic bubble domain materials", AIP Conf. Proc., No. 5, 1972, pp. 240-243.
28. Gianola, U.F., Smith, D.H., Thiele, A.A., and Van Uitert, L.G., "Material requirements for circular magnetic domain devices", IEEE Trans. Magn., vol. MAG-5, Sept. 1969, pp. 558-561.
29. Gorodetsky, G., "Exchange constants in orthoferrites  $YFeO_3$ ", J. Phys. Chem. Solids, vol. 30, July 1969, pp. 1745-1750.
30. Gyorgy, E.M., and Hagedorn, F.B., "Analysis of domain-wall motion in canted antiferromagnets", J. Appl. Phys., vol. 39, Jan. 1968, pp. 88-90.

31. Kooy, C., and Enz, U., "Experimental and theoretical study of the domain configuration in thin layers of  $\text{BaFe}_{12}\text{O}_{19}$ ", Phillips Res. Rep., vol. 151, Feb. 1960, pp. 7-29.
32. Kurtzig, A.J., and Shockley, W., "A new direct measurement of the domain wall energy of the orthoferrites", IEEE Trans. Magn., vol. MAG-4, Sept. 1968, pp. 426-429.
33. Perneski, A.J., "Propagation of cylindrical magnetic domains in orthoferrites", IEEE Trans. Magn., vol. MAG-5, Sept. 1969, pp. 554-557.
34. Robinson, M<sup>C</sup>.D., Bobeck, A.H., and Nielsen, J.W., "Chemical vapor deposition of magnetic garnets for bubble-domain devices", IEEE Trans. Magn., vol. MAG-7, Sept. 1971, pp. 464-466.
35. Rossol, F.C., "Temperature dependence of magnetic domain structure and wall energy in single-crystal Thulium orthoferrite", J. Appl. Phys., vol. 39, Oct. 1968, pp. 5263-5267.
36. Rossol, F.C., "Temperature dependence of rare-earth orthoferrite properties relevant to propagating domain device applications", IEEE Trans. Magn., vol. MAG-5, Sept. 1969, pp. 562-565.
37. Sandfort, R.M., and Burke, E.R., "Logic functions for magnetic bubble devices", IEEE Trans. Magn., vol. MAG-7, Sept. 1971, pp. 358-360.

38. Schick, L.K., Nielsen, J.W., Bobeck, A.H., Kurtzig, A.J., Michaelis, D.C., and Reakstin, J.F., "Liquid phase epitaxial growth of uniaxial garnet films; circuit deposition and bubble propagation", Appl. Phys. Lett., vol. 18, Feb. 1971, pp. 89-91.
39. Sherwood, R.C., Remeika, J.P., and Williams, H.J., "Domain behaviour in some transparent magnetic oxides", J. Appl. Phys., vol. 30, Feb. 1959, pp. 217-225.
40. Sherwood, R.C., Van Uitert, L.G., Wolfe, R., and LeCraw, R.C., "Variation of the reorientation temperature and magnetic crystal anisotropy of the rare-earth orthoferrites", Phys. Lett., vol. 25A, Aug. 1967, pp. 297-298.
41. Smith, D.H., and Anderson, A.W., "The temperature dependence of bubble parameters in some rare-earth garnet films", AIP Conf. Proc., No. 5, 1972, pp. 120-123.
42. Strauss, W., "Detection of cylindrical domains", J. Appl. Phys., vol. 42, Mar. 1971, pp. 1251-1257.
43. Strauss, W., Shumate, Jr., P.W., and Ciak, F.J., "Magneto-resistance sensors for garnet bubble-domains", AIP Conf. Proc., No. 5, 1972, pp. 235-239.
44. Thiele, A.A., "The theory of cylindrical magnetic domains", Bell Syst. Tech. J., vol. 48, Dec. 1969, pp. 3287-3335.

45. Thiele, A.A., "Theory of the static stability of cylindrical domains in uniaxial platelets", J. Appl. Phys., vol. 41, No. 3, March 1970, pp. 1139-1145.
46. Thiele, A.A., "Device implications of the theory of cylindrical magnetic domains", Bell. Syst. Tech. J., vol. 50, Mar. 1971, pp. 725-773.
47. Thiele, A.A., Bobeck, A.H., Della Torre, E., and Gianola, U.G., "The energy and general translation force of cylindrical magnetic domains", Bell Syst. Tech. J., vol. 50, Mar. 1971, pp. 711-724.
48. Treves, D., "Studies on orthoferrites at the Weizmann Institute of Science", J. Appl. Phys., vol. 36, Mar. 1965, pp. 1033-1039.